Engineering Structures 253 (2022) 113761

Contents lists available at ScienceDirect

Engineering Structures

journal homepage: www.elsevier.com/locate/engstruct

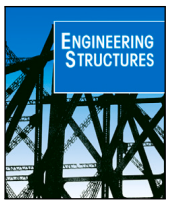

The spatial averaging method for non-homogeneous random fields with application to reliability analysis

Sebastian Geyer [a,*], Iason Papaioannou [a], Lori Graham-Brady [b], Daniel Straub [a]

[a] Engineering Risk Analysis Group, Technische Universität München, Arcisstr. 21, 80290 München, Germany
[b] Department of Civil and Systems Engineering, Johns Hopkins University, 3400 N. Charles St., 21218 Baltimore, MD, USA

ARTICLE INFO

Keywords:
Spatial averaging
Non-homogeneous random fields
Reliability analysis
Spatial variability
Hydraulic structures
Finite elements

ABSTRACT

In probabilistic assessments, inputs with significant spatial variability should be modeled with random fields. Random fields can be non-homogeneous with location-specific marginal distributions, for example, due to site-specific information incorporated through Bayesian analysis or due to spatial trends in the mean or variance of the uncertain quantity. This paper investigates the spatial averaging method for the discretization of non-homogeneous random fields. In this approach, the random field is reduced to a set of random variables representing its local averages over a corresponding set of elemental domains. This is of particular benefit when coupling the random field model with finite elements for structural analysis. We extend the application of the method to non-homogeneous Gaussian and non-Gaussian translation random fields with lognormal, Student's t- and log-Student's t-marginal distribution. The latter two distributions are particularly relevant if spatial data is used in a hierarchical Bayesian random field modeling. Two numerical investigations assess the ability of the method to efficiently represent the response variability and probability of failure of structural systems with spatially variable inputs. The investigations include the effect of different element sizes for the spatial averaging on the system response and applicability of the spatial averaging method to assessing local and global failure modes.

1. Introduction

Many engineering applications require the consideration of physical quantities that vary randomly in space. Common examples include material properties in large structures [1], soil properties in geotechnical sites [2] and the apparent properties of composite materials [3]. Spatially variable properties can be modeled by random fields (RF) [4]. By definition, an RF consists of an infinite number of random variables. Hence, numerical treatment of RFs requires their approximation in terms of a finite number of random variables, a task known as RF discretization. An overview of existing discretization methods can be found in [5] (with focus on the dimensionality reduction aspect) and, more recently, in [6] (with focus on the simulation cost).

The spatial averaging (SA) method expresses the RF through a set of random variables representing local averages of the field over a set of elements. The method was originally proposed by Vanmarcke and Grigoriu [7] and is extensively described in [4]. SA has been applied to homogeneous RFs in various applications and is commonly employed in the context of geotechnical analyses to approximate spatially variable soil properties [8–12]. Such problems have the advantage that geotechnical failure modes are typically dominated by average behavior and not by local extrema of the soil properties. Thus, an RF can often be sufficiently approximated by a small set of random variables or even a single random variable representing the averaging behavior of the RF over a spatial domain (e.g., a failure surface). SA has also been applied to problems in structural analysis to explicitly account for the spatial variability of loads and material properties [7,13–16].

The theory of SA supports the application of the method to non-homogeneous RFs, although it has been reported that it leads to increased numerical effort [17]. SA for non-homogeneous RFs has recently been applied in the context of reliability analysis in [18,19]. Non-homogeneous RFs occur, for example, when the spatial moment functions (mean and variance) follow a trend [e.g.,20,21], or when a homogeneous RF is updated with measurement data through a Bayesian analysis [e.g.,1,22–25]. While in the first case it may be possible to express the RF as function of a homogeneous RF by means of a transformation or standardization [4], this does not hold for the latter case. This paper focuses on the second case, i.e., when the non-homogeneous behavior of the RF results from a Bayesian updating of the RF parameters. Such non-homogeneous RFs are characterized by local changes in the spatial mean function, local reductions of the

* Corresponding author.
E-mail address: s.geyer@tum.de (S. Geyer).

https://doi.org/10.1016/j.engstruct.2021.113761
Received 17 May 2021; Received in revised form 21 September 2021; Accepted 7 December 2021
Available online 7 January 2022

spatial standard deviation function and a complex location-specific autocorrelation structure.

One of the advantages of SA over other RF discretization methods applicable to non-homogeneous RFs is the compact form of the resulting set of averaging random variables. If the RF is Gaussian, the averaging random variables are Gaussian random variables fully defined by a mean vector and a covariance matrix evaluated through spatial integration of the RF moment functions. Hence, it does not require the spectral decomposition of the covariance operator as is the case, e.g., for the Karhunen–Loève expansion [26,27]. Moreover, each of the random variables directly represents the RF in a specific domain. That is, coupling of the method with a finite element model is straightforward, which makes it ideally suited for use in engineering applications [7,13,14]. In addition, the method can account for the fact that the response of structural systems is often determined by regions of high or low values and not by local extrema of random quantities. Last but not least, the illustrative character of the SA random variables can significantly enhance understanding and acceptance of spatial variability and thus increase the motivation in the engineering community for explicit modeling of RFs in engineering assessments. A closely related method, termed local average subdivision tackles the problem by using a hierarchical approach from global to local averaging integrals of RFs to account for spatial variability and the effect of averaging behavior of properties [28]. It was originally developed for homogeneous RFs but can be extended to the general non-homogeneous case.

This paper presents the SA method for non-homogeneous Gaussian RFs following the theory in [4]. In the homogeneous case, the mean is not affected by the averaging operation and, thus, the mean of the spatially averaging random variables equals the mean of the random field. The covariance of the spatially averaging random variables is obtained by integration over the spatial autocorrelation function multiplied by the constant point-variance of the random field [4]. This is not possible for non-homogeneous random fields, where the parameters of the averaging random variables need to be calculated from the spatial mean function and the spatial covariance function. We provide the required expressions for the non-homogeneous case of one- and two-dimensional Gaussian random fields. Furthermore, we extend SA to a special class of non-Gaussian RFs, so-called translation RFs [29], and present application for RF models with lognormal, Student's t- and log-Student's t-marginal distribution. Student's t- and log-Student's t-RFs appear as predictive RFs when learning is performed with spatial data [30]. RFs with lognormal or log-Student's t-marginal distribution are advantageous for modeling non-negative quantities, such as strength parameter of materials, as the support of these distributions is limited to the positive axis.

The focus of the paper is the applicability of the SA method to forward uncertainty propagation and reliability analysis. We investigate the SA method by means of an application to a one-dimensional elastic beam structure with spatially variable beam flexibility. Thereby, we assess the effects of different mesh choices for the RF discretization with SA on the system response and the structural reliability. In a second numerical investigation, the SA method is applied for the reliability analysis of a ship lock chamber wall with spatial data on the concrete friction coefficient. The effect of varying dimension in the SA approximation on the accuracy in representing different failure mechanisms is investigated. On this basis, we conclude with recommendations on the implementation of the SA method for structural reliability analysis.

The remainder of this paper is structured as follows. In Section 2, the spatial averaging method is introduced and explained in detail for the case of one- and two-dimensional Gaussian random fields. An extension to a special class of non-Gaussian random fields can be found in Section 2.3. The presented methodology is illustrated with two numerical examples in Section 3 followed by short conclusions in Section 4.

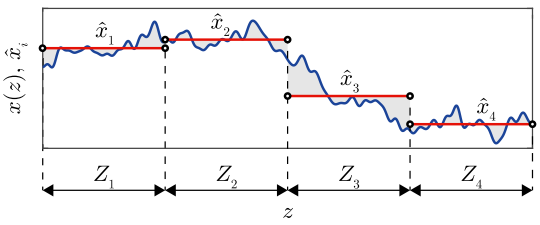

Fig. 1. Random realization of a one-dimensional RF $x(z)$ (blue line) and its approximation with four averaging elements of equal length (red lines, $\hat{x}_i,\ i = 1,\dots,4$). (For interpretation of the references to color in this figure legend, the reader is referred to the web version of this article.)

2. Random field discretization with the spatial averaging method

An RF $X(\boldsymbol{z})$ is defined as a collection of random variables indexed by a continuous spatial coordinate $\boldsymbol{z} \in \boldsymbol{Z}$, where $\boldsymbol{Z} \subset \mathbb{R}^d$ is the spatial domain of definition of the RF, i.e., $d = 1,\ 2$ or 3. An RF is said to be Gaussian if the nth order joint distribution of the random variables corresponding to any collection of points $\boldsymbol{z} = [\boldsymbol{z}_1, \dots, \boldsymbol{z}_n] \in \boldsymbol{Z}$ is a multivariate Gaussian distribution. Gaussian RFs are completely defined by their spatial mean value $\mu_X(\boldsymbol{z})$, their spatial standard deviation $\sigma_X(\boldsymbol{z})$ and their autocorrelation function $\rho(\boldsymbol{z}_i, \boldsymbol{z}_j)$, defining the correlation at two locations $\boldsymbol{z}_i$ and $\boldsymbol{z}_i$ [31]. Any linear mapping of a Gaussian RF is also Gaussian since the Gaussian distribution remains closed under linear transformations [32].

An RF is called homogeneous if its nth order joint PDF is invariant for a shift in $\boldsymbol{z}$, which implies that the marginal PDF $f_X(\boldsymbol{z})$ of the RF and its moments are space-invariant [33]. For Gaussian RFs, homogeneity is implied by homogeneity of the first two moment-functions, i.e., it suffices to know that $\mu_X(\boldsymbol{z})$ and $\sigma_X(\boldsymbol{z})$ are constant in space, i.e., $\mu_X(\boldsymbol{z}) = \mu_X\ \forall\ \boldsymbol{z} \in \boldsymbol{Z}$ and $\sigma_X(\boldsymbol{z}) = \sigma_X\ \forall\ \boldsymbol{z} \in \boldsymbol{Z}$ and that the autocorrelation function $\rho(\boldsymbol{z}_i, \boldsymbol{z}_j)$ can be expressed as $\rho(\boldsymbol{d}_{i,j})$, where $\boldsymbol{d}_{i,j} = \boldsymbol{z}_i - \boldsymbol{z}_j$ is the difference in location of $\boldsymbol{z}_i$ and $\boldsymbol{z}_i$.

The spatial averaging method approximates the RF $X(\boldsymbol{z})$ by a set of random variables $\hat{X}_i,\ i = 1, \dots, n_{SA}$, where each random variable represents the local average of $X(\boldsymbol{z})$ over the domain $\boldsymbol{Z}_i$ defined by the following integral [4]:

$$\hat{X}_i = \frac{I_i}{\Omega_i} = \frac{1}{\Omega_i} \int_{\boldsymbol{Z}_i} X(\boldsymbol{\zeta}) \mathrm{d}\boldsymbol{\zeta}, \tag{1}$$

where Ω_i is the volume of the spatial domain $\boldsymbol{Z}_i$. I_i is the local integral of $X(\boldsymbol{z})$ over the domain $\boldsymbol{Z}_i$. All derivations in this study restrict to one- and two-dimensional RFs but the theoretical approach can be extended to three-dimensional RFs and the general d-dimensional case [4].

Fig. 1 shows a random realization of a one-dimensional RF $x(z)$ in blue and its corresponding realization with an SA discretization of four averaging elements of equal length in red ($\hat{x}_i,\ i = 1, \dots, 4$). Each $\hat{x}_i,\ i = 1, \dots, 4$ represents the average of the RF realization $x(z)$ over the corresponding interval Z_i. Fig. 2 shows a realization of a two-dimensional RF (panel a) and its corresponding realization with an SA discretization of 16 square averaging elements of equal size (panel b). Both figures show that local fluctuations of the RF average out and thus disappear in the SA realization while on a larger scale the spatial variability of the RF is identified and represented. An increasing number of averaging elements results in a more accurate representation of the RF and thus in better representation of local fluctuations. If $X(\boldsymbol{z})$ is a Gaussian RF, the random variables $\hat{X}_i,\ i = 1, \dots, _{SA}$, for the discretization with SA are also Gaussian because of the linearity of the integral operation in Eq. (1). It is possible to use SA for non-Gaussian RFs if the RF can be expressed as function of an underlying Gaussian RF by an isoprobabilistic marginal transformation [29]. Examples of such translation random fields where the transformation is available in closed form are presented in Section 2.3.

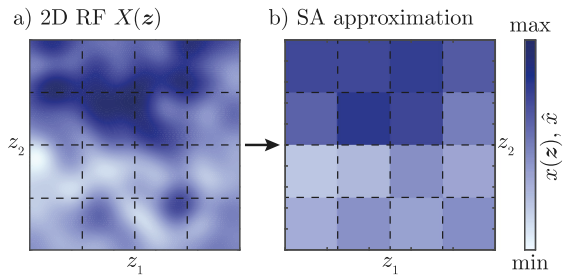

Fig. 2. Random realization of a two-dimensional RF $X(z)$ (panel a) and its SA approximation with 16 square averaging elements of equal size (panel b).

The mean of the random variable $\hat{X}_i$ can be found by integration of the spatial function for the mean $\mu_X(\boldsymbol{z})$ over the averaging domain $\boldsymbol{Z}_i$ [4]:

$$\mu_{\hat{X}_i} = \frac{1}{\Omega_i} \int_{\boldsymbol{Z}_i} \mu_X(\boldsymbol{\zeta})\, \mathrm{d}\boldsymbol{\zeta}. \tag{2}$$

By integration over the spatial autocovariance function $C_X(\boldsymbol{z}_1, \boldsymbol{z}_2)$ the variance of $\hat{X}_i$ can be found [4,18]:

$$\mathrm{Var}\left(\hat{X}_i\right) = \frac{1}{\Omega_i^2} \int_{\boldsymbol{Z}_i} \int_{\boldsymbol{Z}_i} C_X(\boldsymbol{\zeta}_1, \boldsymbol{\zeta}_2)\, \mathrm{d}\boldsymbol{\zeta}_1 \mathrm{d}\boldsymbol{\zeta}_2. \tag{3}$$

The integration in Eq. (2) is d-dimensional, where d is the spatial dimension of $X(\boldsymbol{z})$. Accordingly, the total dimension of the integration in Eq. (3) is $2d$. The covariance of two random variables $\hat{X}_i$ and $\hat{X}_j$ cannot be obtained directly from the autocovariance function. Its derivation is presented for the one- and two-dimensional case in the respective subsections.

If $X(\boldsymbol{z})$ is a homogeneous RF, the mean and variance are constant over $\boldsymbol{Z}$. In this case, the mean is not affected by the averaging integration, i.e., $\mu_{\hat{X}_i} = \mu_X$, $i = 1, \dots, n_{SA}$ and the variance is given as linear function of the RF variance: $\mathrm{Var}\left(\hat{X}_i\right) = \gamma_i \mathrm{Var}(X)$, $i = 1, \dots, n_{SA}$, where γ_i is the variance function representing the average of the autocorrelation function of the field [4,13]. γ_i expresses the reduction in the variance caused by the averaging operation and, hence, decreases with increasing size of the averaging element. It holds that $\gamma_i = 1$ if $\Omega_i = 0$ and $\gamma_i \to 0$ for $\Omega_i \to \infty$ [4,34]. In the homogeneous case, SA underestimates the true variance of the RF in each SA element for $\Omega_i > 0$ [14,35]. This property cannot be directly transferred to the non-homogeneous case on the element level due to a potentially strong fluctuation of the spatial variance function, but remains true in a global view of the RF variability.

For homogeneous RFs, the SA method is extensively described in [4]. This paper focuses on non-homogeneous RFs that have a complex autocorrelation structure and, hence, cannot be transformed into homogeneous RFs.

2.1. Spatial averaging for one-dimensional Gaussian random fields

For the discretization of a one-dimensional RF $X(z)$ with n_{SA} spatially averaging domains, Eqs. (2) and (3) can be rewritten for element i, $i = 1, \dots, n_{SA}$ as follows [4,18]:

$$\mu_{\hat{X}_i} = \frac{1}{L_i} \int_{z_{i_0}}^{z_{i_1}} \mu_X(z)\, \mathrm{d}z, \tag{4}$$

$$\mathrm{Var}\left(\hat{X}_i\right) = \frac{1}{L_i^2} \int_{z_{i_0}}^{z_{i_1}} \int_{z_{i_0}}^{z_{i_1}} C_X(z, z')\, \mathrm{d}z\mathrm{d}z', \tag{5}$$

where z_{i_0} and z_{i_1} denote beginning and end of the averaging domain Z_i and L_i is the length of this domain, i.e., $L_i = z_{i_1} - z_{i_0}$.

The calculation of the covariance of two averaging random variables $\hat{X}_i$ and $\hat{X}_j$ requires four auxiliary lengths L_k, $k = 0, \dots 3$, which are illustrated in Fig. 3 together with the averaging domains Z_i and Z_j.

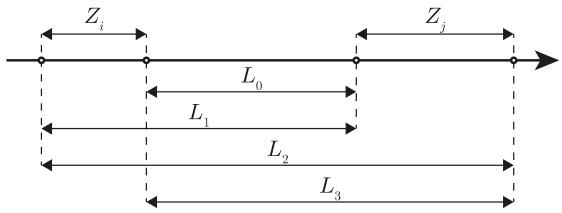

Fig. 3. Lengths L_k, $k = 0, \dots 3$ of the auxiliary intervals for the calculation of the covariance of the random variables $\hat{X}_i$ and $\hat{X}_j$ representing the average behavior of the RF $X(z)$ in the local intervals Z_i and Z_j.

The following algebraic identity can be defined using the local integrals $I_k = \int_{L_k} X(\boldsymbol{\zeta})\mathrm{d}\boldsymbol{\zeta}$, (cf. Eq. (1)) over the illustrated domains [4]:

$$2I_iI_j = I_0^2 - I_1^2 + I_2^2 - I_3^2. \tag{6}$$

Applying the expectation operator on both sides of Eq. (6) gives

$$2\mathrm{E}\left[I_iI_j\right] = \mathrm{E}\left[I_0^2\right] - \mathrm{E}\left[I_1^2\right] + \mathrm{E}\left[I_2^2\right] - \mathrm{E}\left[I_3^2\right]. \tag{7}$$

Taking the expectation of the individual terms in Eq. (6) results in [4]

$$2\mathrm{E}\left[I_i\right]\mathrm{E}\left[I_j\right] = \mathrm{E}^2\left[I_0\right] - \mathrm{E}^2\left[I_1\right] + \mathrm{E}^2\left[I_2\right] - \mathrm{E}^2\left[I_3\right]. \tag{8}$$

Subtracting Eq. (8) from Eq. (7) gives the following expression for the covariance of I_i and I_j:

$$C\left(I_i, I_j\right) = \frac{1}{2}\Big(\mathrm{Var}\left(I_0\right) - \mathrm{Var}\left(I_1\right) + \mathrm{Var}\left(I_2\right) - \mathrm{Var}\left(I_3\right)\Big). \tag{9}$$

The covariance of $\hat{X}_i$ and $\hat{X}_j$ can be calculated making use of their proportionality to I_i and I_j defined in Eq. (1):

$$C\left(\hat{X}_i, \hat{X}_j\right) = \frac{C\left(I_i, I_j\right)}{L_iL_j}. \tag{10}$$

Using Eq. (9), one gets [4,18]:

$$C\left(\hat{X}_i, \hat{X}_j\right) = \frac{1}{2L_iL_j} \sum_{k=0}^{3} (-1)^k\, \Delta\left(Z_k\right), \tag{11}$$

where $\Delta\left(Z_k\right)$ is given by

$$\Delta\left(Z_k\right) = L_k^2 \mathrm{Var}\left(\hat{X}_k\right). \tag{12}$$

When $Z_j = Z_i$, Eq. (11) simplifies to $L_0 = L_2 = L_i$ and $L_1 = L_3 = 0$ (cf. Fig. 3). Accordingly, $\Delta\left(Z_0\right) = \Delta\left(Z_2\right) = L_i^2\mathrm{Var}\left(\hat{X}_i\right)$ and $\Delta\left(Z_1\right) = \Delta\left(Z_3\right) = 0$ and hence Eq. (11) reduces to Eq. (5). The random variables $\hat{X}_i$, $i = 1, \dots n_{SA}$ are Gaussian random variables and thus the discretization of $X(z)$ is fully defined by the mean vector $\boldsymbol{\mu}_{\hat{X}}$ containing the individual mean values $\mu_{\hat{X}_i}, i = 1, \dots n$ and the covariance matrix $\mathbf{C}_{\hat{X}}$, where $C_{\hat{X}}(i, j), i = 1, \dots n_{SA}$, $j = 1, \dots n_{SA}$ is given by the covariance of $\hat{X}_i$ and $\hat{X}_j$.

2.2. Spatial averaging for two-dimensional Gaussian random fields

Let $X(\boldsymbol{z})$ be a two-dimensional Gaussian RF, where $\boldsymbol{z} \in \boldsymbol{Z}$ describes a position in the two-dimensional domain $\boldsymbol{Z}$. SA proceeds by dividing $\boldsymbol{Z}$ into n_{SA} rectangular elements with edges parallel to the coordinate axes z_1 and z_2. Expressions for the mean and variance of the random variables $\hat{X}_i$, $i = 1, \dots n_{SA}$ representing the average of $X(\boldsymbol{z})$ in the ith element can be found from Eqs. (2) and (3) [4]:

$$\mu_{\hat{X}_i} = \frac{1}{A_i} \int_{z_{2,i_0}}^{z_{2,i_1}} \int_{z_{1,i_0}}^{z_{1,i_1}} \mu_X(z_1, z_2)\, \mathrm{d}z_1\mathrm{d}z_2, \tag{13}$$

$$\mathrm{Var}\left(\hat{X}_i\right) = \frac{1}{A_i^2} \int_{z_{2,i_0}}^{z_{2,i_1}} \int_{z_{2,i_0}}^{z_{2,i_1}} \int_{z_{1,i_0}}^{z_{1,i_1}} \int_{z_{1,i_0}}^{z_{1,i_1}} C_X(z_1, z_2; z_1', z_2')\, \mathrm{d}z_1\mathrm{d}z_1'\mathrm{d}z_2\mathrm{d}z_2', \tag{14}$$

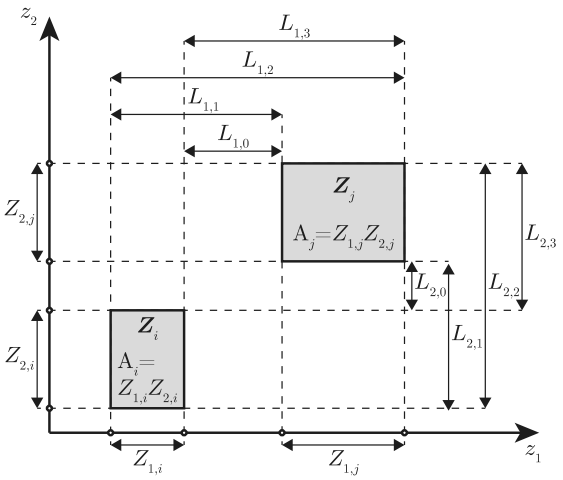

Fig. 4. Edges $L_{1,k}$ and $L_{2,l}$ of the auxiliary domains $\boldsymbol{Z}_{kl}$, $k = 0, \dots 3$, $l = 0, \dots 3$ for calculating the covariance of the random variables $\hat{X}_i$ and $\hat{X}_j$ representing the average behavior of the RF $X(\boldsymbol{z})$ in the rectangular domains $\boldsymbol{Z}_i$ and $\boldsymbol{Z}_j$.

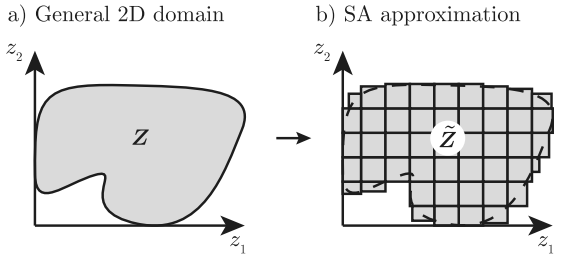

Fig. 5. Approximation of a non-rectangular two-dimensional domain $\boldsymbol{Z}$ by an enveloping domain $\tilde{\boldsymbol{Z}}$ consisting of rectangular elements of variable size.

where $A_i = Z_{1,i} Z_{2,i}$ denotes the area of the averaging domain. $Z_{1,i}$ and $Z_{2,i}$ are the lengths of the edges in z_1, z_2 respectively, i.e., $Z_{1,i} = z_{1,i_1} - z_{1,i_0}$ and $Z_{2,i} = z_{2,i_1} - z_{2,i_0}$.

Eqs. (6) to (11) can be extended to the two-dimensional case (cf. Fig. 4) to obtain the following expression for the covariance of two averaging random variables $\hat{X}_i$ and $\hat{X}_j$ [4]:

$$C\left(\hat{X}_i, \hat{X}_j\right) = \frac{1}{4 A_i A_j} \sum_{k=0}^{3} \sum_{l=0}^{3} (-1)^k (-1)^l \Delta\left(Z_{1,k}, Z_{2,l}\right), \tag{15}$$

where A_i and A_j denote the areas of $\boldsymbol{Z}_i$ and $\boldsymbol{Z}_j$, which are the averaging domains for $\hat{X}_i$ and $\hat{X}_j$. $\Delta\left(Z_{1,k}, Z_{2,l}\right)$ is defined as

$$\Delta\left(Z_{1,k}, Z_{2,l}\right) = A_{kl}^2 \mathrm{Var}\left(\hat{X}_{kl}\right). \tag{16}$$

$A_{kl} = L_{1,k} L_{2,l}$ is the area of the rectangular auxiliary domain $\boldsymbol{Z}_{kl}$, $k = 0, \dots, 3$, $l = 0, \dots, 3$. Fig. 4 shows the averaging domains $\boldsymbol{Z}_i$ and $\boldsymbol{Z}_j$ and the edges of the auxiliary domains. The random variables $\hat{X}_i$, $i = 1, \dots n_{SA}$ are Gaussian random variables. Hence, similar to the one-dimensional case, the mean vector $\boldsymbol{\mu}_{\hat{X}}$ and covariance matrix $\mathbf{C}_{\hat{X}}$ of the random variables $\hat{X}_i$, $i = 1, \dots n_{SA}$, are sufficient to discretize $X(\boldsymbol{z})$.

Eqs. (13) to (15) are only applicable for rectangular averaging elements. If the domain $\boldsymbol{Z}$ cannot be divided into rectangular averaging domains, it needs to be approximated by such a domain [4]. An example is shown in Fig. 5, where $\boldsymbol{Z}$ is approximated by the enveloping domain $\tilde{\boldsymbol{Z}}$. A prescribed degree of accuracy for the approximation can be achieved by adjusting the size of the rectangular elements and, if necessary, introducing a rotation of the coordinate system. The studies in this paper are restricted to the case where $\boldsymbol{Z}$ can be divided into rectangular averaging elements.

2.3. Spatial averaging for non-Gaussian translation random fields

Although, in theory, the SA method is applicable to non-Gaussian RFs, in practice, the derived equations for the parameters of the averaging random variables are only sufficient in the Gaussian case. For most other cases it is difficult or even impossible to find all required expressions for obtaining a complete probabilistic description of the resulting RVs $\hat{X}_i$ [14]. However, it is possible to extend the applicability of the method to the class of so-called translation RFs, given by the following marginal transformation [32,36]:

$$X(\boldsymbol{z}) = T\left(U(\boldsymbol{z})\right). \tag{17}$$

$U(\boldsymbol{z})$ is a zero-mean and unit-variance Gaussian RF with autocorrelation coefficient function $\rho_U(\boldsymbol{z}, \boldsymbol{z}')$. The mapping of Eq. (17) is designed to preserve a given marginal cumulative distribution function (CDF) $F_X(x)$ of the RF $X(\boldsymbol{z})$. Given that $F_X(x)$ is strictly increasing, $T(\cdot)$ can be defined as $T(\cdot) = F_X^{-1}(\Phi(\cdot))$, where $F_X^{-1}(\cdot)$ denotes the inverse CDF of $X(\boldsymbol{z})$ and $\Phi(\cdot)$ is the standard normal CDF [37]. $U(\boldsymbol{z})$ can be obtained from $X(\boldsymbol{z})$ by inversion of Eq. (17), i.e., $U(\boldsymbol{z}) = T^{-1}(X(\boldsymbol{z}))$. Note that, in order to approximate the RF with a set of Gaussian random variables, the spatial correlation needs to be modeled for the underlying Gaussian RF. Three special cases of translation RFs, for which $T(\cdot)$ is given by an analytic expression, are presented in the following. The equations are given for a single averaging element over the entire domain of definition but can be generalized by dividing $\boldsymbol{Z}$ into subdomains and applying the Equations for mean and covariance derived for the Gaussian case.

2.3.1. Lognormal random field

In contrast to a Gaussian RF, a lognormal RF can be used to model non-negative quantities, which makes it preferable, e.g., for modeling mechanical properties. Consider an RF $Y(\boldsymbol{z})$ on the domain $\boldsymbol{Z}$ defined by the following function of a zero-mean and unit-variance Gaussian RF $U(\boldsymbol{z})$:

$$Y(\boldsymbol{z}) = \exp\Big(U(\boldsymbol{z}) \cdot \sigma_X(\boldsymbol{z}) + \mu_X(\boldsymbol{z})\Big) = \exp\Big(X(\boldsymbol{z})\Big). \tag{18}$$

$X(\boldsymbol{z})$ is a Gaussian RF with mean function $\mu_X(\boldsymbol{z})$ and standard deviation function $\sigma_X(\boldsymbol{z})$. F_Y at any $\boldsymbol{z} \in \boldsymbol{Z}$ is a lognormal distribution, with parameters $\mu_{\ln Y}(\boldsymbol{z}) = \mu_X(\boldsymbol{z})$ and $\sigma_{\ln Y}(\boldsymbol{z}) = \sigma_X(\boldsymbol{z})$:

$$Y(\boldsymbol{z}) \sim \log\mathcal{N}\left(\mu_{\ln Y}(\boldsymbol{z}), \sigma_{\ln Y}(\boldsymbol{z})\right). \tag{19}$$

Spatial averaging is then performed for $X(\boldsymbol{z})$ resulting in a Gaussian random variable $\hat{X}_{\boldsymbol{Z}}$ with parameters $\mu_{\hat{X}}$ and $\sigma_{\hat{X}} = \sqrt{\mathrm{Var}\left(\hat{X}_{\boldsymbol{Z}}\right)}$ given by Eqs. (2) and (3). Applying the transformation of Eq. (18) gives

$$\hat{Y}_{\boldsymbol{Z}} = \exp\left(\frac{1}{\Omega_{\boldsymbol{Z}}} \int_{\boldsymbol{Z}} X(\boldsymbol{\zeta}) \mathrm{d}\boldsymbol{\zeta}\right) = \exp\left(\hat{X}_{\boldsymbol{Z}}\right), \tag{20}$$

where $\hat{Y}_{\boldsymbol{Z}}$ is a lognormal distributed random variable with parameters $\mu_{\ln\hat{Y}} = \mu_{\hat{X}}$ and $\sigma_{\ln\hat{Y}} = \sigma_{\hat{X}}$. Due to the non-linear transformation, $\hat{Y}_{\boldsymbol{Z}}$ does not represent the arithmetic average but the geometric average of $Y(\boldsymbol{z})$ over $\boldsymbol{z}$. It is noted that the geometric average is always smaller than or equal to the arithmetic average. Hence, using the geometric average for the SA discretization of a lognormal RF provides a lower bound on the spatial average of the RF. While this is reasonable and conservative for some modeling cases (e.g., for low-strength dominated soil properties [e.g.,9,10]), it may provide a non-appropriate approximation of the true RF when the RF represents a load/demand on the structure [e.g.,11].

2.3.2. Student's t-random field

The Student's t-distribution can be used to model a Gaussian quantity accounting for the uncertainty in the parameters of the Gaussian distribution [e.g.,38]. Consider a Student's t-RF $Y(\boldsymbol{z})$, in which F_Y at any $\boldsymbol{z} \in \boldsymbol{Z}$ is a Student's t-distribution, with location parameter $\mu_Y(\boldsymbol{z})$, scale parameter $\sigma_Y(\boldsymbol{z})$ and degrees of freedom ν_Y [30,38,39]:

$$Y(\boldsymbol{z}) \sim \mathcal{T}\left(\mu_Y(\boldsymbol{z}), \sigma_Y(\boldsymbol{z}), \nu_Y\right). \tag{21}$$

Note that ν_Y is space-invariant. The transformation of Eq. (17) is given as [39]

$$Y(\boldsymbol{z}) = \sqrt{\frac{\nu_Y}{\chi}}\Big(U(\boldsymbol{z}) \cdot \sigma_Y(\boldsymbol{z})\Big) + \mu_Y(\boldsymbol{z}) = \sqrt{\frac{\nu_Y}{\chi}} X(\boldsymbol{z}) + \mu_Y(\boldsymbol{z}), \tag{22}$$

where $X(\boldsymbol{z})$ is a zero-mean Gaussian RF with standard deviation $\sigma_X(\boldsymbol{z}) = \sigma_Y(\boldsymbol{z})$ and χ is a random variable that follows the χ^2 distribution with ν_Y degrees of freedom. As only $X(\boldsymbol{z})$ and the function for the mean value $\mu_Y(\boldsymbol{z})$ are subject to spatial variability, the spatial average $\hat{Y}_Z$ over the domain $\boldsymbol{Z}$ can be expressed by the following averaging integral:

$$\begin{aligned}\hat{Y}_Z &= \frac{1}{\Omega_Z}\int_Z Y(\boldsymbol{\zeta})\mathrm{d}\boldsymbol{\zeta} = \frac{1}{\Omega_Z}\int_Z \sqrt{\frac{\nu_Y}{\chi}} X(\boldsymbol{\zeta}) + \mu_Y(\boldsymbol{\zeta})\mathrm{d}\boldsymbol{\zeta} \\ &= \frac{\sqrt{\frac{\nu_Y}{\chi}}}{\Omega_Z}\int_Z X(\boldsymbol{\zeta})\mathrm{d}\boldsymbol{\zeta} + \frac{1}{\Omega_Z}\int_Z \mu_Y(\boldsymbol{\zeta})\mathrm{d}\boldsymbol{\zeta} \\ &= \sqrt{\frac{\nu_Y}{\chi}}\hat{X}_Z + \mu_{\hat{Y}},\end{aligned} \tag{23}$$

where $\hat{X}_Z$ is a zero-mean Gaussian random variable with variance calculated according to Eq. (3) and $\mu_{\hat{Y}}$ is the mean of the spatial average of $Y(\boldsymbol{z})$ over $\boldsymbol{Z}$ as defined in Eq. (2).

2.3.3. Log-Student's t-random field

The log-Student's t-distribution combines the lognormal and the Student's t-distribution and thus, can be used to model non-negative quantities accounting for parameter uncertainty [30]. Consider a log-Student's t-RF $V(\boldsymbol{z})$, i.e., F_V at any $\boldsymbol{z} \in \boldsymbol{Z}$ is a log-Student's t-distribution [30,40]:

$$V(\boldsymbol{z}) \sim \ln\mathcal{T}\left(\mu_{\ln V}(\boldsymbol{z}), \sigma_{\ln V}(\boldsymbol{z}), \nu_V\right). \tag{24}$$

The parametrization of F_V is done by means of the parameters of the underlying Student's t-distribution. At any $\boldsymbol{z} \in \boldsymbol{Z}$ it holds that $Y(\boldsymbol{z}) = \ln(V(\boldsymbol{z}))$ follows a Student's t-distribution with location parameter $\mu_Y(\boldsymbol{z}) = \mu_{\ln V}(\boldsymbol{z})$, scale parameter $\sigma_Y(\boldsymbol{z}) = \sigma_{\ln V}(\boldsymbol{z})$ and degrees of freedom $\nu_Y = \nu_V$ [30]. By combining Eqs. (18) and (22), the transformation of Eq. (17) is given as follows:

$$\begin{aligned}V(\boldsymbol{z}) &= \exp\left(\sqrt{\frac{\nu_V}{\chi}} \cdot \left(U(\boldsymbol{z}) \cdot \sigma_{\ln V}(\boldsymbol{z})\right) + \mu_{\ln V}(\boldsymbol{z})\right) \\ &= \exp\left(\sqrt{\frac{\nu_V}{\chi}} X(\boldsymbol{z}) + \mu_{\ln V}(\boldsymbol{z})\right).\end{aligned} \tag{25}$$

$X(\boldsymbol{z})$ is a zero-mean Gaussian RF with standard deviation $\sigma_X(\boldsymbol{z}) = \sigma_{\ln V}(\boldsymbol{z})$ and χ is a random variable that follows the χ^2 distribution with ν_V degrees of freedom. The spatial average $\hat{V}_Z$ over the domain $\boldsymbol{Z}$ can be calculated as follows:

$$\begin{aligned}\hat{V}_Z &= \exp\left(\frac{1}{\Omega_Z}\int_Z Y(\boldsymbol{\zeta})\mathrm{d}\boldsymbol{\zeta}\right) \\ &= \exp\left(\frac{\sqrt{\frac{\nu_V}{\chi}}}{\Omega_Z}\int_Z X(\boldsymbol{\zeta})\mathrm{d}\boldsymbol{\zeta} + \frac{1}{\Omega_Z}\int_Z \mu_{\ln V}(\boldsymbol{\zeta})\mathrm{d}\boldsymbol{\zeta}\right) \\ &= \exp\left(\sqrt{\frac{\nu_V}{\chi}}\hat{X}_Z + \mu_{\ln\hat{V}}\right).\end{aligned} \tag{26}$$

$\hat{X}_Z$ is a zero-mean Gaussian random variable with variance calculated according to Eq. (3) and $\mu_{\ln\hat{V}}$ is the mean of the spatial average of $\ln(V(\boldsymbol{z})) = Y(\boldsymbol{z})$ over $\boldsymbol{Z}$. Similar to the lognormal RF in Section 2.3.1, $\hat{V}_Z$ represents the geometric average of $V(\boldsymbol{z})$ over $\boldsymbol{Z}$ instead of the arithmetic average.

3. Numerical investigations

In this Section, the accuracy of the SA method for approximating non-homogeneous RFs is investigated by means of two numerical investigations. The non-homogeneity of the RFs in both cases stems from the combination of a homogeneous prior RF with measurement data. The first investigation is a one-dimensional beam under uniform load with spatially variable beam flexibility analyzed in a statically determinate setting with analytical solution and a statically indeterminate setting where the system response is evaluated using a finite element model. Different SA settings regarding element size and number are investigated for different output quantities of the structural system. The second investigation is a sliding failure mechanism in a ship lock chamber wall where the friction coefficient in a construction joint is modeled as a two-dimensional RF. Two different failure mechanisms are considered and the effect of the chosen SA discretization on the reliability estimates is analyzed.

3.1. Measures for the accuracy of the random field discretization

Discretizing an RF $X(\boldsymbol{z})$ with a finite number of random variables $\hat{X}_i$, $i = 1, \dots n$, yields an approximation error. If the $\hat{X}_i$, $i = 1, \dots n$, are used for uncertainty propagation through a numerical model, this error typically propagates through the model and is reflected in the model response. However, depending on the type of the quantity of interest, the error in the model response may be larger or smaller than the error in the RF approximation [24]. The point-wise approximation error is defined as the difference of the quantity of interest Q and its approximation $\hat{Q}$ at spatial location $\boldsymbol{z}$, i.e., $\varepsilon(\boldsymbol{z}) = Q(\boldsymbol{z}) - \hat{Q}(\boldsymbol{z})$. Based on $\varepsilon(\boldsymbol{z})$, numerous local and global error measures can be defined to assess the accuracy of an RF discretization. e.g., the bias, error variance or mean-square error [e.g., 5,32,41]. The latter two include the covariance of $Q(\boldsymbol{z})$ and $\hat{Q}(\boldsymbol{z})$, which can require the numerical solution of a complex integral equation. In addition, their interpretation is not always straightforward and hence they are not further discussed here. Instead, we use the normalized bias $\varepsilon_\mu(\boldsymbol{z})$ and the normalized variance error $\varepsilon_{\mathrm{V}}(\boldsymbol{z})$ as point-wise error measures in this study. They are defined as [24]

$$\varepsilon_\mu(\boldsymbol{z}) = \frac{\mathrm{E}\left[Q(\boldsymbol{z})\right] - \mathrm{E}\left[\hat{Q}(\boldsymbol{z})\right]}{\mathrm{E}\left[Q(\boldsymbol{z})\right]}, \tag{27}$$

$$\varepsilon_{\mathrm{V}}(\boldsymbol{z}) = \frac{\mathrm{Var}\left(Q(\boldsymbol{z})\right) - \mathrm{Var}\left(\hat{Q}(\boldsymbol{z})\right)}{\mathrm{Var}\left(Q(\boldsymbol{z})\right)}. \tag{28}$$

Taking the weighted integral of Eqs. (27) and (28) over the domain $\boldsymbol{Z}$ yields the corresponding global error measures [41]:

$$\bar{\varepsilon}_\mu = \frac{1}{\Omega}\int_Z \left|\varepsilon_\mu(\boldsymbol{z})\right| \,\mathrm{d}\boldsymbol{z}, \tag{29}$$

$$\bar{\varepsilon}_{\mathrm{V}} = \frac{1}{\Omega}\int_Z \left|\varepsilon_{\mathrm{V}}(\boldsymbol{z})\right| \,\mathrm{d}\boldsymbol{z}. \tag{30}$$

In addition, the influence of the RF discretization on the system response is assessed in terms of the system reliability, or equivalently its probability of failure. The failure event F is expressed in terms of a limit state function $g\big(X(\boldsymbol{z})\big)$, such that failure occurs if $g\big(X(\boldsymbol{z})\big) \leq 0$. That is, the probability of failure is $P_F = \Pr\Big(g\big(X(\boldsymbol{z})\big) \leq 0\Big)$. We will be comparing P_F with $\hat{P}_F = \Pr\Big(g\big(\hat{X}(\boldsymbol{z})\big) \leq 0\Big)$. Typically, $g\big(X(\boldsymbol{z})\big)$ is a function of an output quantity of interest $Q(\boldsymbol{z})$ and F occurs with a small probability. Hence, through assessing the influence of the RF discretization on the probability of failure, we evaluate the ability of the discretization to accurately represent the tails of the distribution of $Q(\boldsymbol{z})$.

3.2. Analysis of a one-dimensional beam

A one-dimensional beam subject to uniformly distributed vertical load is investigated, whose flexibility $F(z)$ is modeled by a Gaussian RF that is updated with measurement data. The beam has length $L = 2\,\mathrm{m}$ and the applied load is $q = 1.4\,\mathrm{kN\,m^{-1}}$. $\hat{F}(z)$ is the piece-wise constant SA approximation of $F(z)$ by using n_{SA} averaging elements. Euler–Bernoulli beam theory is used to evaluate the response of the structural system. We consider two different settings for the boundary conditions of the beam; a statically determinate case and a statically indeterminate case.

3.2.1. Random field model of the beam flexibility

The prior model of $F(z)$ is a homogeneous RF with a mean of $\mu'_F = 0.5\,\mathrm{MN}^{-1}\,\mathrm{m}^{-2}$ and a standard deviation of $\sigma'_F = 0.1\,\mathrm{MN}^{-1}\,\mathrm{m}^{-2}$. The prior autocorrelation function is modeled by the exponential correlation function [31]:

$$\rho'(z_i, z_j) = \exp\left(-\frac{2\left|z_j - z_i\right|}{\vartheta}\right), \tag{31}$$

where ϑ is the scale of fluctuation, which is set to 1 m.

We assume that measurement data $\mathbf{M}$ is available in the form of n_m direct measurements of the beam flexibility $\boldsymbol{x}_m = [x_{m,1}, \ldots, x_{m,n_m}]$ and the corresponding measurement locations $\boldsymbol{z}_m = [z_{m,1}, \ldots, z_{m,n_m}]$. These measurements are associated with an additive zero-mean Gaussian measurement error ϵ with standard deviation $\sigma_\epsilon^2 = 0.05\mu'_F$. In this case, updating of $F(z)$ can be done in closed form by making use of the self-conjugacy of the Gaussian distribution, resulting in the following posterior mean and covariance functions [1,4,23]:

$$\mu''_F(z) = \mu'_F + \boldsymbol{R}_{\boldsymbol{z}_m}(z) \cdot \mathbf{R}^{-1}_{\boldsymbol{z}_m,\epsilon} \cdot \left(\boldsymbol{x}_m - \mu'_F\right)^{\mathsf{T}}, \tag{32}$$

$$C''_F\left(z_i, z_j\right) = \left(\sigma'_F\right)^2 \cdot \left(\rho(z_i, z_j) - \boldsymbol{R}_{\boldsymbol{z}_m}(z_i) \cdot \mathbf{R}^{-1}_{\boldsymbol{z}_m,\epsilon} \cdot \boldsymbol{R}^{\mathsf{T}}_{\boldsymbol{z}_m}(z_j)\right). \tag{33}$$

$\boldsymbol{R}_{\boldsymbol{z}_m}(z)$ is a $1 \times n_m$ row vector function with element i equal to $\rho'(z, z_{m,i})$. $\mathbf{R}_{\boldsymbol{z}_m,\epsilon} = \mathbf{R}_{\boldsymbol{z}_m,\boldsymbol{z}_m} + \mathbf{R}_\epsilon$, where $\mathbf{R}_{\boldsymbol{z}_m,\boldsymbol{z}_m}$ is an $n_m \times n_m$ matrix with element (i, j) equal to $\rho'(z_{m,i}, z_{m,j})$ and $\mathbf{R}_\epsilon = \left(\frac{\sigma_\epsilon}{\sigma'_F}\right)^2 \cdot \mathrm{I}$, where I is the $n_m \times n_m$ identity matrix.

A single measurement $f_m = 0.75 \cdot \mu'_F = 0.375\,\mathrm{MN}^{-1}\,\mathrm{m}^{-2}$ at measurement location $z_m = 0.25L = 0.5\,\mathrm{m}$ is considered in the RF update. The resulting posterior RF parameters of the beam flexibility are obtained by application of Eqs. (32) and (33). We first set the number of SA elements to $n_{SA} = 4$. Fig. 6 illustrates the posterior RF parameters together with the parameters of the corresponding four spatial averaging random variables calculated by means of Eqs. (4), (5) and (11). The measurement leads to a reduction in the mean value at the measurement location and in the region around the measurement compared to the prior mean (blue line in panel a). In addition, the uncertainty and hence the standard deviation at the measurement location and in its vicinity is reduced (blue line in panel b). These effects decrease with increasing distance from the measurement location and thus the posterior parameters converge to the prior parameters. A similar effect can be observed in the posterior correlation structure (panel c). The parameters of the spatial averaging random variables reflect the non-homogeneity, however the local extrema in the spatial mean and standard deviation average out when applying the averaging operations for the discretization with SA (red lines in panel a and b). The spatial autocorrelation function of the RF is approximated by a 4×4 correlation matrix (panel d). Again, the SA discretization accounts for the non-homogeneity of the RF but local effects average out.

3.2.2. Statically determinate cantilever beam

The statically determinate cantilever beam is illustrated in Fig. 7. The internal forces are independent of the flexibility and hence the bending moment $M(z)$ can be directly calculated as $M(z) = -\frac{q}{2}(L - z)^2$. Using the Euler–Bernoulli beam theory, the rotation $\varphi(z)$ and vertical displacement $w(z)$ as illustrated in Fig. 7 are obtained as follows:

$$\varphi(z) = -\frac{q}{2}\int_0^z (L - t)^2\, F(t)\,\mathrm{d}t, \tag{34}$$

$$w(z) = -\frac{q}{2}\int_0^z \int_0^s (L - t)^2\, F(t)\,\mathrm{d}t\mathrm{d}s. \tag{35}$$

Since $F(z)$ is modeled with a Gaussian RF and $\varphi(z)$ and $w(z)$ are linear functions of $F(z)$, they are also Gaussian RFs. Based on Eqs. (34) and (35), spatial functions for the mean and autocovariance of the system response RFs can be derived:

$$\mu_\varphi(z) = -\frac{q}{2}\int_0^z (L - t)^2\, \mu_F(t)\,\mathrm{d}t, \tag{36}$$

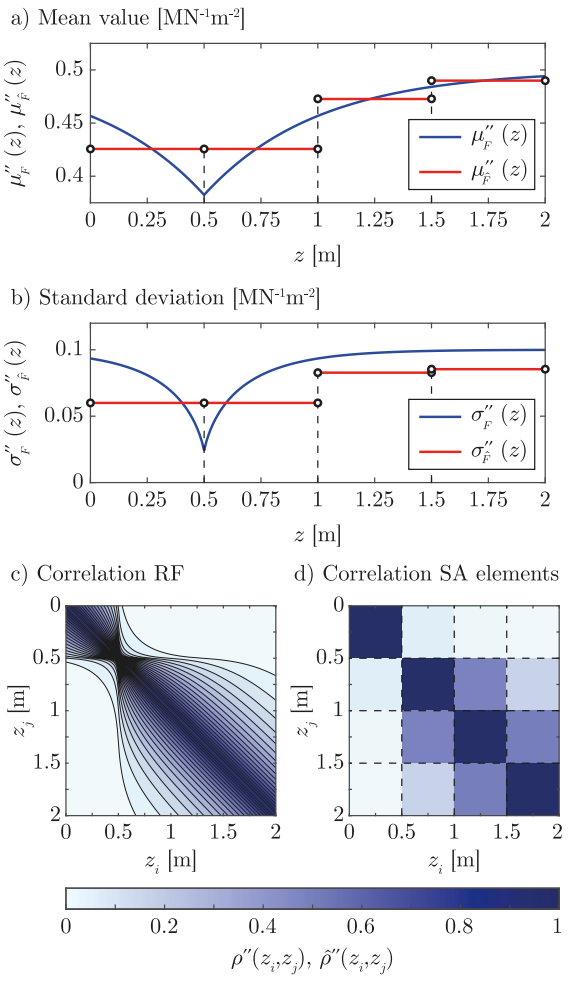

Fig. 6. Posterior spatial mean value (panel a) and standard deviation (panel b) of the RF for the beam flexibility $F''(z)$ (blue) and its approximation with four averaging elements $\hat{F}''(z)$ (red); posterior spatial autocorrelation of the RF $F''(z)$ (panel c) and correlation of the four averaging random variables for the approximation of $F''(z)$ with SA (panel d). (For interpretation of the references to color in this figure legend, the reader is referred to the web version of this article.)

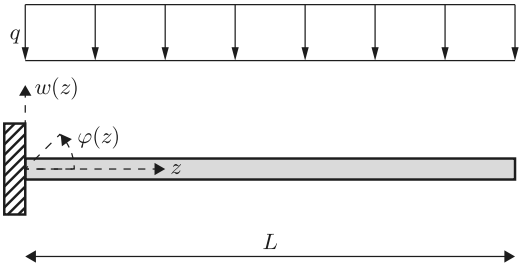

Fig. 7. Statically determinate cantilever beam under uniform vertical load q.

$$C_\varphi(z_i, z_j) = \frac{q^2}{4}\int_0^{z_j}\int_0^{z_i} \left(L - t_i\right)^2 \left(L - t_j\right)^2 C_F(t_i, t_j)\,\mathrm{d}t_i\mathrm{d}t_j, \tag{37}$$

$$\mu_w(z) = -\frac{q}{2}\int_0^z \int_0^s (L - t)^2\, \mu_F(t)\,\mathrm{d}t\mathrm{d}s, \tag{38}$$

$$C_w(z_i, z_j) = \frac{q^2}{4}\int_0^{z_j}\int_0^{z_i}\int_0^{s_j}\int_0^{s_i} \left(L - t_i\right)^2 \left(L - t_j\right)^2 \times C_F(t_i, t_j)\,\mathrm{d}t_i\mathrm{d}t_j\mathrm{d}s_i\mathrm{d}s_j. \tag{39}$$

Replacing $\mu_F(t)$ and $C_F(t_i, t_j)$ in Eqs. (36) to (39) with the element-wise constant approximations obtained by means of Eqs. (4) and (11)

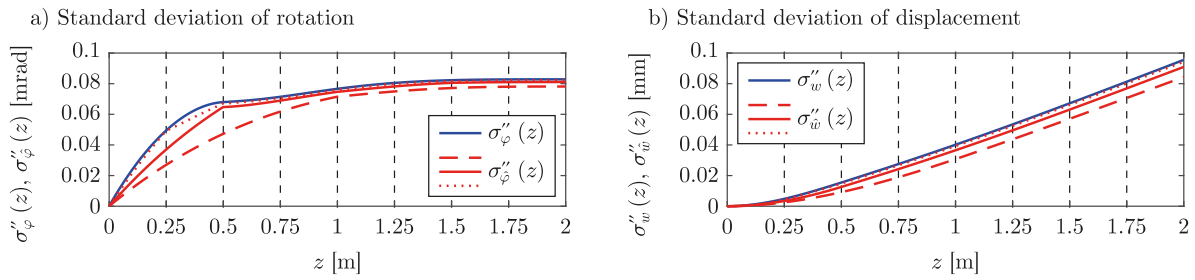

Fig. 8. Posterior spatial standard deviation of the system response (rotation: panel a; displacement: panel b) for the cantilever beam. The blue lines mark the analytical RF solution and the red lines mark the SA approximation with $n_{SA} = 2$ (dashed line), 4 (solid line) and 8 (dotted line). (For interpretation of the references to color in this figure legend, the reader is referred to the web version of this article.)

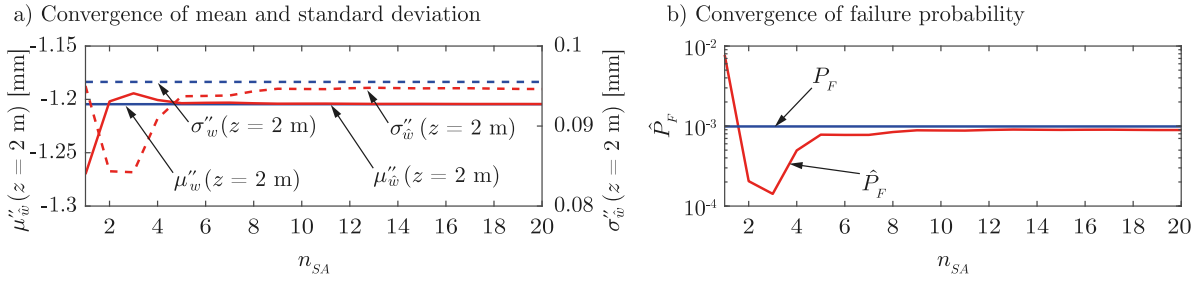

Fig. 9. Panel a shows the SA approximation of the mean (solid red line, left ordinate) and standard deviation (dashed red line, right ordinate) for the tip displacement of the cantilever beam as function of the number of equisized averaging elements n_{SA}. The blue lines show the analytical mean value $\mu''_w(z = 2\,\mathrm{m})$ (solid blue line) and standard deviation $\sigma''_w(z = 2\,\mathrm{m})$ (dashed blue line). Panel b shows the corresponding SA approximation of the failure probability $\hat P_F$ (red line) as function of the number of equisized averaging elements n_{SA}. The blue line shows the analytical failure probability P_F. (For interpretation of the references to color in this figure legend, the reader is referred to the web version of this article.)

Table 1
Average normalized bias $\bar\varepsilon_\mu$ and variance error $\bar\varepsilon_V$ of the beam rotation φ'' and vertical displacement w'' for varying number of spatial averaging elements n_{SA} to discretize the posterior beam flexibility RF.

n_{SA}	$\bar\varepsilon_\mu$		$\bar\varepsilon_V$	
	φ''	w''	φ''	w''
2	0.009	0.019	0.301	0.458
4	0.010	0.020	0.144	0.240
8	0.003	0.005	0.044	0.063

results in $\mu_{\hat\varphi}(z)$, $C_{\hat\varphi}(z_i, z_j)$, $\mu_{\hat w}(z)$ and $C_{\hat w}(z_i, z_j)$, i.e., the spatial functions for the system response when $F(z)$ is approximated by $\hat F(z)$ with n_{SA} spatial averaging elements. Due to the linearity of the averaging operations, $\hat\varphi(z)$ and $\hat w(z)$ are also Gaussian RFs. The system response RFs and their SA discretization with $n_{SA} = 2$, 4 and 8 are evaluated using Eqs. (36) to (39). The spatial mean value is approximated well with any chosen SA discretization. For $n_{SA} = 2$, the maximum of the point-wise error $\varepsilon_\mu(z)$ is in the order of 5% (close to the fixed end of the beam) and <1% for most spatial locations z. $\varepsilon_\mu(z)$ decreases further for $n_{SA} = 4$ and $n_{SA} = 8$. In general, $\varepsilon_\mu(z)$ decreases with increasing distance to the fixed end. Fig. 8 shows the spatial standard deviation of the beam rotation (panel a) and vertical displacement (panel b). The spatial standard deviation of the system response RFs is underestimated throughout the length of the beam, with decreasing approximation error for increasing n_{SA}. The local effect of the measurement appears in the shape of $\sigma''_\varphi(z)$ and $\sigma''_{\hat\varphi}(z)$ but not in $\sigma''_w(z)$ and $\sigma''_{\hat w}(z)$ due to the smoothing caused by the additional integration when calculating the vertical displacement.

The average error measures for the system response according to Eqs. (29) and (30) are listed in Table 1 for $n_{SA} = 2$, 4 and 8. The average bias is small for all configurations and the variance error decreases with increasing n_{SA}. In general, the average error is larger for the displacement than it is for the rotation.

To investigate the effect of the SA discretization on the failure probability of the system, a maximum allowable vertical displacement of $w_{\lim} = -1.5\,\mathrm{mm}$ is defined. Since the vertical displacement of a cantilever beam reaches its maximum at the free end, the following limit state function can be formulated:

$$g(F(z)) = w''(z = 2\,\mathrm{m}) - w_{\lim}, \tag{40}$$

Replacing $w''(z = 2\,\mathrm{m})$ by $\hat w''(z = 2\,\mathrm{m})$ in Eq. (40) yields the SA approximation of the failure event. Both $w''(z = 2\,\mathrm{m})$ and $\hat w''(z = 2\,\mathrm{m})$ are Gaussian random variables with mean value and standard deviation directly computable by means of Eqs. (38) and (39). Thus, P_F is given as

$$P_F = \Phi\left(\frac{w_{\lim} - \mu''_w(z = 2\,\mathrm{m})}{\sigma''_w(z = 2\,\mathrm{m})}\right), \tag{41}$$

where $\Phi(\cdot)$ is the cumulative distribution function of the standard normal distribution. The reference solution is $P_F = 9.9 \times 10^{-4}$. The SA approximation of P_F is obtained by replacing $\mu''_w(z = 2\,\mathrm{m})$ and $\sigma''_w(z = 2\,\mathrm{m})$ by the respective SA approximations.

Fig. 9 illustrates the approximated mean and standard deviation of the displacement at the free end and the corresponding failure probability estimate as function of n_{SA} and compares them to the respective analytical solutions. It appears that a single averaging element results in a strong overestimation of the failure probability as $\hat P_F$ is approximately eight times larger than P_F. When increasing n_{SA}, $\hat P_F$ becomes negatively biased and converges to the analytical solution P_F with increasing n_{SA}. The relative error in the probability of failure falls below 30% for $n_{SA} \geq 5$. The overestimation for $n_{SA} = 1$ results from the fact that the RF $F''(z)$ is discretized with a single random variable that averages over the whole length of the beam, which reduces the local effect of the measurement at $z_m = 0.5\,\mathrm{m}$ and leads to an overestimation of the flexibility in that region. This error propagates through the model evaluation and, on the one hand, leads to a strong bias of the vertical displacement. On the other hand, it leads to an almost perfect approximation of $\sigma''_w(z = 2\,\mathrm{m})$ with a single averaging element, since it counteracts the underestimation of the variance that is typically observed when using a small number of averaging elements.

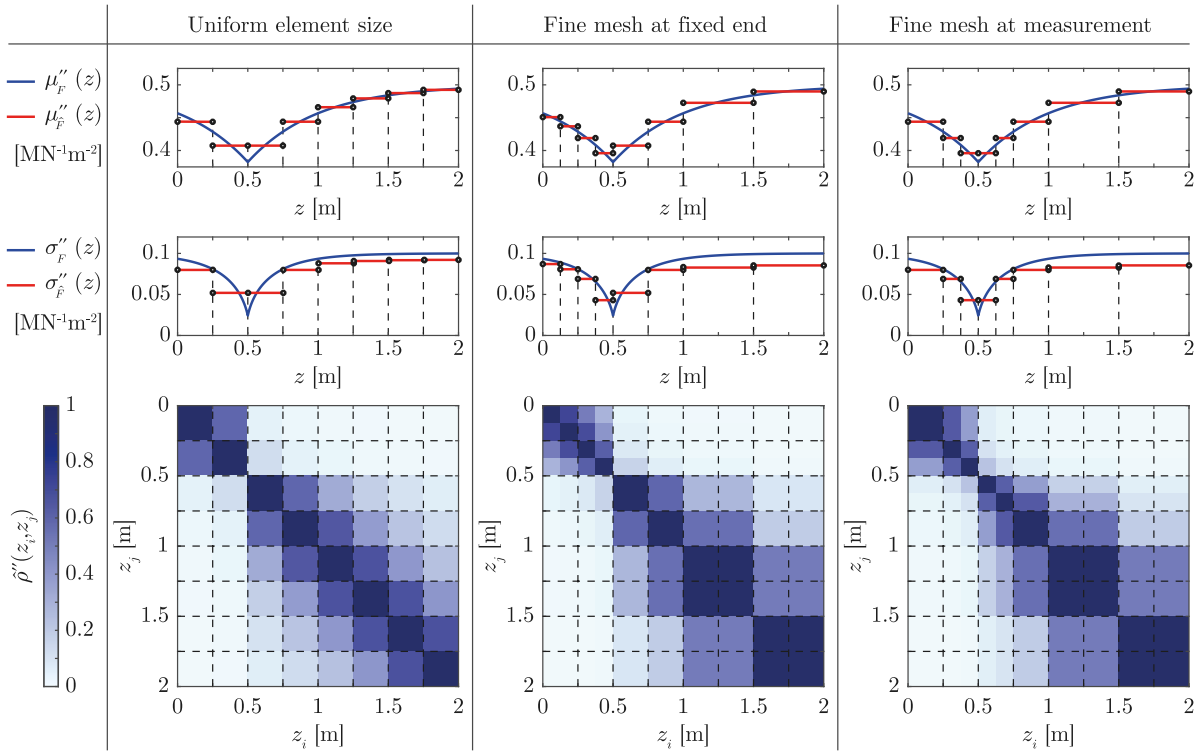

Fig. 10. Posterior mean value (top row), standard deviation (middle row) and correlation (bottom row) of the SA approximation of the posterior flexibility RF with eight equisized averaging elements (left column), refined mesh at the fixed end (middle column) and refined mesh at the measurement location z_m (right column). (For interpretation of the references to color in this figure legend, the reader is referred to the web version of this article.)

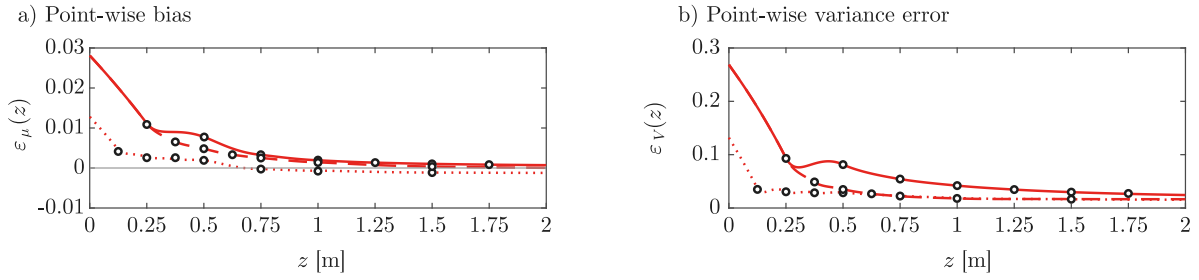

Fig. 11. Effect of adaptive SA element size in an 8-element mesh (solid line: equisized elements, dotted line: refined mesh at the fixed end, dashed line: refined mesh around the measurement location) on the point-wise normalized bias (panel a) and variance error (panel b) of the vertical displacement.

So far, the SA elements have been equisized, i.e., $L_i = \frac{L}{n_{SA}}, i = 1, \ldots, n_{SA}$ independent of the location within the structural system. In the following, the SA mesh is chosen such that it is finer in regions that may be critical for the system response, in this case the fixed end of the beam $z = 0\,\text{m}$ and the measurement location $z_m = 0.5\,\text{m}$. Fig. 10 shows the parameters of the random variables and their correlation for $n_{SA} = 8$ with equisized elements (left column), refined mesh at the fixed end (middle column) and refined mesh around the measurement location $z_m = 0.5\,\text{m}$ (right column). As $n_{SA} = 8$ for all three settings, a refinement of the SA mesh in one region of the beam necessarily leads to a coarser mesh in other parts of the domain, in this case towards the free end of the beam. Fig. 11 illustrates the effect on the point-wise error in approximating the vertical displacement.

Refining the mesh leads to smaller bias and variance error in that region compared to the error with equisized elements. The coarser mesh towards the free end of the beam leads to slightly larger bias and variance error for the two adaptive mesh choices. The average error measures are listed in Table 2 showing the minor effect on the average variance error of the vertical displacement. The investigated adaptive mesh choices lead to a failure probability estimate of $\hat{P}_F = 9.6 \times 10^{-4}$ (mesh refinement at fixed end) and $\hat{P}_F = 9.0 \times 10^{-4}$ (mesh refinement at measurement location), respectively compared to $\hat{P}_F = 8.4 \times 10^{-4}$ with $n_{SA} = 8$ equisized averaging elements. It is reminded that the reference solution is $P_F = 9.9 \times 10^{-4}$. However, although the results with the adaptive mesh choices are more accurate, they are also more sensitive to the analysis at hand and thus should be handled with caution. This sensitivity is illustrated by using another adaptive SA mesh with $n_{SA} = 8$, where the refinement is towards the free end of the beam, i.e., the region of interest with respect to the limit state function of Eq. (40). The SA mesh is a left-to-right reversion of the adaptive SA mesh with the refinement at the fixed end (cf. middle column of

Table 2
Average normalized bias $\bar{\varepsilon}_\mu$ and variance error $\bar{\varepsilon}_V$ of the vertical displacement w'' and estimated probability of failure $\hat{P}_F$ with eight SA elements of uniform size, a refined mesh at the fixed end and a refined mesh at the measurement location.

	$\bar{\varepsilon}_\mu$	$\bar{\varepsilon}_V$	$\hat{P}_F$
Uniform mesh	0.005	0.063	8.4×10^{-4}
Fine mesh at fixed end	0.001	0.025	9.6×10^{-4}
Fine mesh at z_m	0.004	0.044	9.0×10^{-4}

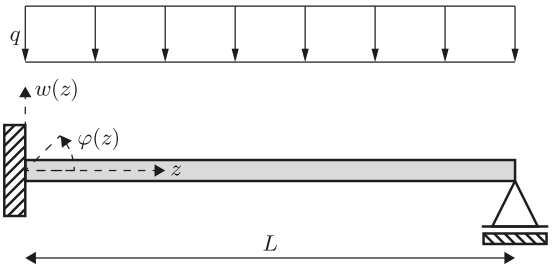

Fig. 12. Statically indeterminate propped cantilever beam under uniform vertical load q.

Table 3
Average normalized bias $\bar{\varepsilon}_\mu$ and variance error $\bar{\varepsilon}_V$ of the propped cantilever vertical displacement w'' for varying number of spatial averaging elements n_{SA} to discretize the posterior beam flexibility RF.

n_{SA}	$\bar{\varepsilon}_\mu$	$\bar{\varepsilon}_V$
2	0.016	0.322
4	0.023	0.278
8	0.007	0.070

Fig. 10). The resulting failure probability estimate is $\hat{P}_F = 5.0 \times 10^{-4}$, which underestimates P_F significantly. In the general case, it might be difficult to find a suitable adaptive SA mesh, especially in cases where the relation between the RF discretization and the output quantity of interest is hidden by a black box model evaluation, as is the case for complex finite element models.

3.2.3. Propped cantilever beam

The structural system is modified by adding an additional vertical support at the free end of the beam as illustrated in Fig. 12. The resulting propped cantilever beam is statically indeterminate and thus, Eqs. (34) and (35) cannot be used to evaluate the beam rotation and displacement.

Due to the spatial variability of the beam flexibility, the inner forces of the beam depend on the flexibility. Therefore, the system response is evaluated with the linear finite element method based on the Euler–Bernoulli beam theory with a finite element size of $l_{FE} = 0.01\,\mathrm{m}$. Since the system response RFs and their moments cannot be calculated analytically, a numerical reference solution is employed. To this end, the posterior flexibility RF is discretized with the Karhunen–Loève (KL) expansion with a large number of terms ($m_{KL} = 500$) [27]. The KL expansion is based on a spectral decomposition of the auto-covariance operator of the RF and can be used for homogeneous and non-homogeneous RFs [1,24,41]. Using the KL expansion, the mean value of an RF is represented exactly, while there is an approximation error in the covariance operator. The average variance error of the beam flexibility with the chosen number of terms for the reference solution is smaller than 1%. The parameters of the posterior flexibility RF $F''(z)$ are the same as in the previous investigation and its SA discretization is done with four equisized averaging elements (cf. Fig. 6). The reference solution as well as the SA solution for the moments of the vertical displacement are obtained by running a Monte Carlo simulation with $N_{MCS} = 1 \times 10^4$ independent samples and is illustrated in Fig. 13.

Panel a shows that the mean displacement is approximated well with four SA elements, concerning both shape and magnitude of the curve. The standard deviation of the displacement is underestimated throughout the beam and the magnitude increases with increasing distance to one of the supports.

Table 3 lists the average bias and variance error of the vertical displacement for $n_{SA} = 2$, 4 and 8. Increasing n_{SA} to eight elements leads to large error reductions while the difference between $n_{SA} = 2$ and $n_{SA} = 4$ is comparatively small. Comparison of Table 3 with Table 1 for the statically determinate cantilever beam indicates that the average error is larger for the propped cantilever beam than for the statically determinate cantilever beam.

Due to the non-uniform flexibility of the propped cantilever beam, the inner forces (i.e., bending moment and shear) are functions of the applied load and the support reactions, which need to be evaluated numerically, e.g., by means of the finite element method. The bending moment in a propped cantilever beam is calculated as follows:

$$M(z) = M(z=0) \cdot \frac{L-z}{L} + q \cdot \left(L \cdot \frac{z}{2} - \frac{z^2}{2} \right), \tag{42}$$

where $M(z=0)$ is the bending moment at the fixed end of the beam. For constant beam flexibility, the support reactions can be determined analytically and $M(z=0) = -q \cdot \frac{L^2}{8}$. As $F(z)$ is modeled by an RF, the evaluated bending moment at the fixed end depends on the chosen discretization. To illustrate this, a reliability analysis with the following limit state function is performed:

$$g(F(z)) = M(z = 0\,\mathrm{m}) - M_{\mathrm{lim}}, \tag{43}$$

where M_{lim} is chosen as $-1.25 \cdot q \cdot \frac{L^2}{8} = -750\,\mathrm{kN\,m}$. It is noted that $M(z = 0\,\mathrm{m})$ is not a Gaussian random variable and thus, evaluation of the probability of failure in terms of the normal integral is not possible. Instead, a Monte Carlo simulation with $N_{MCS} = 1 \times 10^6$ samples is employed to estimate P_F, where the full finite element model of the propped cantilever beam is evaluated for each realization of the beam flexibility. A reference solution is obtained based on the KL expansion with $m_{KL} = 500$ terms to discretize the beam flexibility in a Monte Carlo simulation with $N_{MCS} = 1{\times}10^7$ resulting in $P_F = 2.01{\times}10^{-3}$. The results for varying number of averaging elements in the SA discretization are illustrated in Fig. 14. The SA approximations for mean (red line) and standard deviation (dashed red line) are plotted as function of n_{SA} in panel a and compared to the respective reference solution (blue line and dashed blue line). If $n_{SA} = 1$, the beam flexibility is uniform throughout the domain, leading to a deterministic bending moment at the fixed end ($\hat{\mu}''_M(z=0) = -q \cdot \frac{L^2}{8} = -600\,\mathrm{kN\,m}$ and $\hat{\sigma}''_M(z=0) = 0\,\mathrm{kN\,m}$). The SA method underestimates both mean $\hat{\mu}''_M(z=0)$ and standard deviation $\hat{\sigma}''_M(z=0)$ before converging to the reference solution with increase of n_{SA}. Panel b shows the convergence of the estimated failure probability $\hat{P}_F$ (red line) towards the reference solution (blue line). Failure cannot occur for $n_{SA} = 1$ because the uniform flexibility results in a deterministic bending moment that does not lead to a failed state of the system. No failure sample was observed for $n_{SA} = 2$ in the Monte Carlo simulation with the chosen sample size, indicating that $\hat{P}_F$ strongly underestimates P_F. Choosing $n_{SA} \geq 3$ leads to negatively biased estimates of the failure probability converging towards the reference solution with increasing n_{SA}. $\hat{P}_F$ is of the correct order of magnitude for $n_{SA} \geq 5$.

3.2.4. Summary and interpretation of results

The one-dimensional beam example shows that SA can be used to approximate non-homogeneous RFs in reliability analyses of simple beam structures. Due to the smoothing effect of the forward operator, local fluctuations in the beam flexibility average out and thus, the system response can be approximated well with spatially averaging elements. Not surprisingly, a larger number of averaging elements and thus, a larger number of random variables to approximate the RF leads to a better global accuracy of the system response approximation. However, due to the changing interval bounds when changing the number of SA elements, this does not necessarily hold for all error measures when the RF is non-homogeneous. The distribution tails of the system response are especially important when performing reliability analysis. Our results show that the distribution tails can be sufficiently well approximated with a reasonable number of random variables for the RF discretization, although the required number is larger than for estimating the mean response. The choice of an adaptive size of the averaging elements can lead to a better accuracy of the results, but at

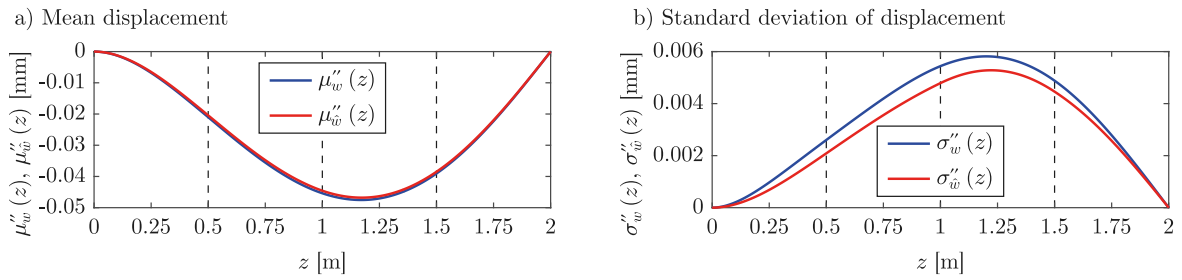

Fig. 13. Posterior spatial mean value (panel a) and standard deviation (panel b) of the vertical displacement for the propped cantilever beam. The KL expansion in the reference solution (blue) discretizes the RF $F''(z)$ with $m_{KL} = 500$ terms, the SA approximation (red) with four averaging elements of equal size. (For interpretation of the references to color in this figure legend, the reader is referred to the web version of this article.)

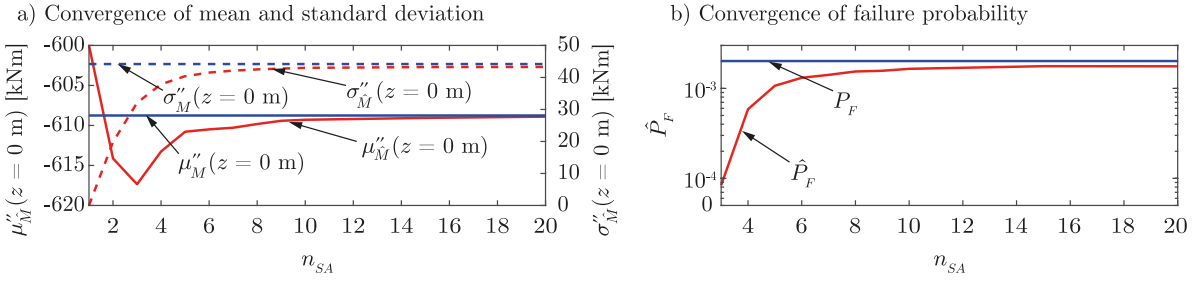

Fig. 14. Panel a shows the SA approximation of the mean (solid red line, left ordinate) and standard deviation (dashed red line, right ordinate) for the bending moment at the fixed end of the propped cantilever beam as function of the number of equisized averaging elements n_{SA}. The blue lines show the analytical mean value $\mu''_M(z = 0\,\mathrm{m})$ (solid blue line) and standard deviation $\sigma''_M(z = 0\,\mathrm{m})$ (dashed blue line). Panel b shows the corresponding SA approximation of the failure probability $\hat{P}_F$ (red line) as function of the number of equisized averaging elements n_{SA}. The blue line shows the analytical failure probability P_F.. (For interpretation of the references to color in this figure legend, the reader is referred to the web version of this article.)

the same time increases the sensitivity of the SA discretization to the behavior of the numerical model. Hence, it cannot be recommended for general use; in general problems, the underlying numerical model may be more complex, in which case the choice of an appropriate adaptive mesh is not straightforward. The influence of the spatial variability of the beam flexibility on the system response depends on the quantity of interest and the problem setting. Local failure mechanisms (in our investigation the bending moment) require a larger number of averaging elements than failure mechanisms dominated by global behavior of the flexibility (in our investigation the maximum displacement). Other than in statically determinate settings, the inner forces in a statically indeterminate setting are influenced by spatially variable beam flexibility and thus are spatially variable functions. This leads to larger approximation error in the spatial system response when using SA for the RF discretization.

3.3. Sliding failure in the construction joint of a shiplock

The chamber of a fictitious ship lock is investigated. It has a length of $L = 109\,\mathrm{m}$, a usable width between the chamber walls of 12 m and is made of unreinforced tamped concrete. Several failure mechanisms can occur in a ship lock, one of them being sliding of the construction joint between the chamber wall and the base slab. The cross section of the wall including the joint with a width of $W = 4.5\,\mathrm{m}$ and the surrounding soil are illustrated in Fig. 15. In structural verifications, sliding of this joint due to shear is one of the failure mechanisms that are investigated by checking the following condition [42,43]:

$$V_{Ed} \leq S_{Rd}, \tag{44}$$

where V_{Ed} denotes the applied design shear force at the interface and S_{Rd} is the design sliding resistance of the joint. In practice, both V_{Ed} and S_{Rd} depend on a number of factors and additional variables to cover different effects on the sliding failure. For simplicity, a slimmed-down version is used here. V_{Ed} consists of all forces acting horizontally on the structure, i.e., the horizontal earth and water pressure. S_{Rd} is

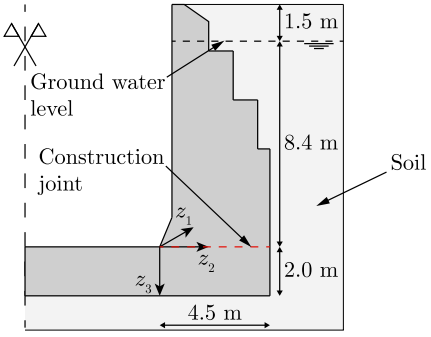

Fig. 15. Half cross section of a ship lock chamber with construction joint between base slab and chamber wall.

the product of the vertical forces N_{Ed} and the friction coefficient τ of the construction joint. Further contributions to S_{Rd} (e.g., the concrete tensile strength) are neglected at this point. N_{Ed} is given by the self weight of the chamber wall plus the vertical earth and water pressure, wall friction and crack and pore water pressure.

In this example, two failure events are considered. The first one is a local exceedance of the sliding resistance along z_2, defined by the following limit state function:

$$g_1(z_1, \tau(\boldsymbol{z})) = \gamma_R \cdot S_R(z_1) - V_E(z_1), \tag{45}$$

where $\gamma_R = 1.3$ is a deterministic coefficient to account for the spatial load bearing behavior of the chamber wall in a simplified manner. A detailed mechanical model for the spatial load bearing would go beyond the scope of the investigation at this point. $S_R(z_1)$ is defined as the average sliding resistance along the construction joint in z_2:

$$S_R(z_1) = \frac{N_E(z_1)}{4.5\,\mathrm{m}} \int_{0\,\mathrm{m}}^{4.5\,\mathrm{m}} \tau(\boldsymbol{z})\, \mathrm{d}z_2. \tag{46}$$

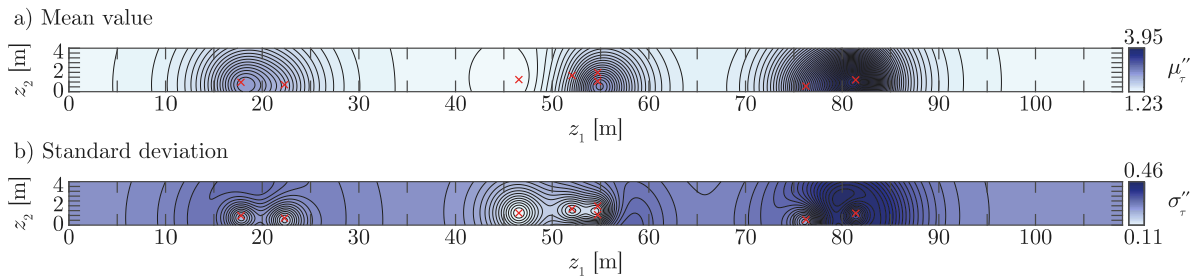

Fig. 16. Posterior spatial mean value (panel a) and standard deviation (panel b) of the two-dimensional RF for the friction coefficient in the construction joint of a ship lock chamber wall. The red crosses indicate the locations of the $n_m = 8$ measurements of the friction coefficient. (For interpretation of the references to color in this figure legend, the reader is referred to the web version of this article.)

$V_E(z_1)$ and $N_E(z_1)$ are the loads acting on the structure in horizontal and vertical direction. The second limit state function is defined as exceedance of the average sliding resistance of a substantial part of the chamber wall:

$$g_2(\zeta_1, \tau(\boldsymbol{z})) = \int_{\zeta_1 - \frac{\bar{z}_1}{2}}^{\zeta_1 + \frac{\bar{z}_1}{2}} S_R(z_1)\,\mathrm{d}z_1 - \int_{\zeta_1 - \frac{\bar{z}_1}{2}}^{\zeta_1 + \frac{\bar{z}_1}{2}} V_E(z_1)\,\mathrm{d}z_1, \tag{47}$$

where $\bar{z}_1 = \frac{L}{5}$ is the length in z_1 that is assumed critical for the sliding failure mechanism of a substantial part of the wall and $\zeta_1 \in (\frac{\bar{z}_1}{2}, L - \frac{\bar{z}_1}{2})$ is the location of the potential failure point along the wall.

Failure of the chamber wall occurs if any of the two described limit state functions gives a value smaller than zero at any point in z_1 direction. Thus, the limit state function for system failure is given as a function of the two individual failure probabilities:

$$g_{\mathrm{sys}}(\tau(\boldsymbol{z})) = \min \begin{Bmatrix} \min_{z_1} \left\{ g_1(z_1, \tau(\boldsymbol{z})) \right\},\ z_1 \in (0\,\mathrm{m}, L) \\ \min_{\zeta_1} \left\{ g_2(\zeta_1, \tau(\boldsymbol{z})) \right\},\ \zeta_1 \in (\frac{\bar{z}_1}{2}, L - \frac{\bar{z}_1}{2}) \end{Bmatrix}. \tag{48}$$

3.3.1. Two-dimensional random field for the friction coefficient

The friction coefficient τ in the construction joint is modeled by a two-dimensional RF $\tau(\boldsymbol{z})$ in z_1 and z_2. The prior RF $\tau'(\boldsymbol{z})$ is homogeneous with lognormal marginal distribution F'_τ. The corresponding parameters are $\mu'_{\ln\tau}$ and $\sigma'_{\ln\tau}$, which are the mean value and standard deviation of the Gaussian distribution $F'_{\ln\tau}$ of the underlying homogeneous Gaussian RF $\tau_{\ln}(\boldsymbol{z})$. The spatial correlation of $\tau'_{\ln}(\boldsymbol{z})$ is modeled with the Matérn correlation model with a smoothness parameter of $\nu = 1.5$ [31,44]:

$$\rho'(\boldsymbol{z}_i, \boldsymbol{z}_j) = \left(1 + \frac{\sqrt{3}\delta_z}{l_c}\right) \cdot \exp\left(-\frac{\sqrt{3}\delta_z}{l_c}\right). \tag{49}$$

The correlation length is chosen as $l_c = 4\,\mathrm{m}$.

A typical assumption for the friction coefficient in indented construction joints of concrete structures is $\tau = 0.9$ [42], while in-situ measurements often show significantly higher friction coefficients. Hence, the prior RF distribution parameters are chosen such that $\tau = 0.9$ approximately equals the 5%-quantile value of the lognormal distribution. This is achieved by choosing $\mu'_{\ln\tau} = 0.25$ and $\sigma'_{\ln\tau} = 0.2$. The corresponding mean value and standard deviation are $\mu'_\tau = 1.31$ and $\sigma'_\tau = 0.26$. Note that this prior distribution is based on relatively strong assumptions and may not hold in practice.

It is assumed that data from concrete core samples of the chamber wall is available including $n_m = 8$ spatial measurements of the friction coefficient τ in the construction joint (i.e., $z_3 = 0\,\mathrm{m}$). Table 4 lists the measurements $\boldsymbol{\tau}_m = [\tau_{m,1}, \ldots, \tau_{m,8}]$ and corresponding locations. It is further assumed that the data are associated with a lognormal multiplicative measurement error with median 1 and coefficient of variation $\mathrm{CV}_\varepsilon = 0.1$, which is equivalent to an additive zero-mean Gaussian measurement error for the logarithmic transformation of the measurements $\ln(\boldsymbol{\tau}_m)$. Eqs. (32) and (33) can be adapted for the two-dimensional update of the mean and covariance function of the Gaussian RF $\tau_{\ln}(\boldsymbol{z})$:

$$\mu''_{\ln\tau}(\boldsymbol{z}) = \mu'_{\ln\tau} + \boldsymbol{R}_{\boldsymbol{z}_m}(\boldsymbol{z}) \cdot \mathbf{R}^{-1}_{\boldsymbol{z}_m,\varepsilon} \cdot \left(\ln(\boldsymbol{\tau}_m) - \mu'_{\ln\tau}\right)^{\mathsf{T}}, \tag{50}$$

Table 4
Measurement values τ_m of the friction coefficient and corresponding locations in the construction joint of the ship lock chamber wall.

	1	2	3	4	5	6	7	8
z_1 [m]	17.80	22.30	46.55	52.05	54.70	54.70	76.25	81.40
z_2 [m]	0.75	0.50	1.25	1.45	0.85	1.75	0.35	1.00
τ_m	2.6	2.1	1.2	1.7	3.1	2.1	2.9	5.0

$$C''_{\ln\tau}(\boldsymbol{z}_i, \boldsymbol{z}_j) = \left(\sigma'_{\ln\tau}\right)^2 \cdot \left(\rho(\boldsymbol{z}_i, \boldsymbol{z}_j) - \boldsymbol{R}_{\boldsymbol{z}_m}(\boldsymbol{z}_i) \cdot \mathbf{R}^{-1}_{\boldsymbol{z}_m,\varepsilon} \cdot \boldsymbol{R}^{\mathsf{T}}_{\boldsymbol{z}_m}(\boldsymbol{z}_j)\right). \tag{51}$$

$\boldsymbol{R}_{\boldsymbol{z}_m}(z)$ is a $1 \times n_m$ row vector function with element i equal to $\rho'(\boldsymbol{z}, \boldsymbol{z}_{m,i})$. $\mathbf{R}_{\boldsymbol{z}_m,\varepsilon} = \mathbf{R}_{\boldsymbol{z}_m,\boldsymbol{z}_m} + \mathbf{R}_\varepsilon$, where $\mathbf{R}_{\boldsymbol{z}_m,\boldsymbol{z}_m}$ is an $n_m \times n_m$ matrix with element (i, j) equal to $\rho'(\boldsymbol{z}_{m,i}, \boldsymbol{z}_{m,j})$ and $\mathbf{R}_\varepsilon = \sigma^2_{\ln\varepsilon} \cdot \mathrm{I}$, where I is the $n_m \times n_m$ identity matrix. The resulting posterior mean value and standard deviation of the marginal lognormal distributions of $\tau''(\boldsymbol{z})$ are plotted in Fig. 16.

To approximate $\tau''(\boldsymbol{z})$ with SA, the domain of the construction joint is divided into rectangular averaging domains. Their length is $\frac{L}{n_{SA,1}}$ in z_1 and $\frac{W}{n_{SA,2}}$ in z_2, resulting in $n_{SA} = n_{SA,1} \cdot n_{SA,2}$ rectangular elements of equal size. The corresponding parameters of the lognormal averaging random variables and their correlation are found by application of Eqs. (13) to (15) in combination with the transformation in Eq. (20). The mean values and standard deviations for $n_{SA,1} = 20$ and $n_{SA,2} = 1$ are illustrated in Fig. 17. It can be seen that local extrema of the RF parameters resulting from high or low measurement values are not fully reflected in the SA parameters but regions of high or low values are visible.

3.3.2. Loads acting on the structure

The vertical forces from self weight, vertical earth and water pressure, wall friction and crack and pore water pressure are modeled space-invariant and deterministically. They sum up to $N_E(z_1) = 580\,\mathrm{k\,N\,m^{-1}}$ per running length. The horizontal water pressure is assumed deterministic based on the given ground water level (cf. Fig. 15), resulting in a value of $V_{E,w} = 353\,\mathrm{kN\,m^{-1}}$ per running length. The horizontal earth pressure consists of a basic value of $V_{E,e} = 159\,\mathrm{kN\,m^{-1}}$ and is multiplied with a location-specific random term. This term is modeled with a one-dimensional KL representation using a fixed number of terms ($m_{KL} = 10$). It has mean value $\mu_p = 1$, standard deviation $\sigma_p = 0.05$ and exponential spatial correlation (cf. Eq. (31)) with a scale of fluctuation of $\vartheta = 40\,\mathrm{m}$.

3.3.3. Reliability analysis

The reliability analysis is carried out with MCS using 10^7 independent samples. A reference solution is obtained by discretizing the two-dimensional RF $\tau''(\boldsymbol{z})$ with the KL expansion with $m_{KL} = 500$ terms. Fig. 18 illustrates the resulting failure probability estimates as function of the number of SA elements in z_1 direction $n_{SA,1}$. Panel a shows that $\hat{P}_F$ (red line) strongly underestimates P_F (blue line) for small $n_{SA,1}$ but converges to the reference solution with increasing $n_{SA,1}$. $\hat{P}_F = 0$ when $n_{SA,1} < 4$, confirming the trend to underestimate

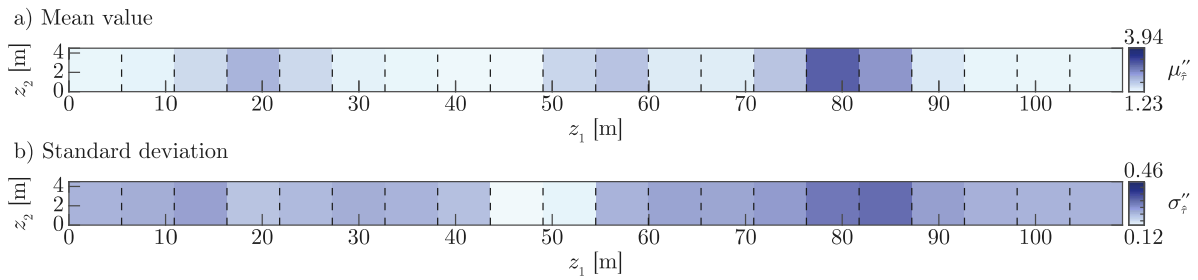

Fig. 17. Posterior spatial mean value (panel a) and standard deviation (panel b) of the SA discretization of the two-dimensional RF for the friction coefficient in the construction joint of a ship lock chamber wall. The number of elements is $n_{SA} = 20$ with $n_{SA,1} = 20$ and $n_{SA,2} = 1$.

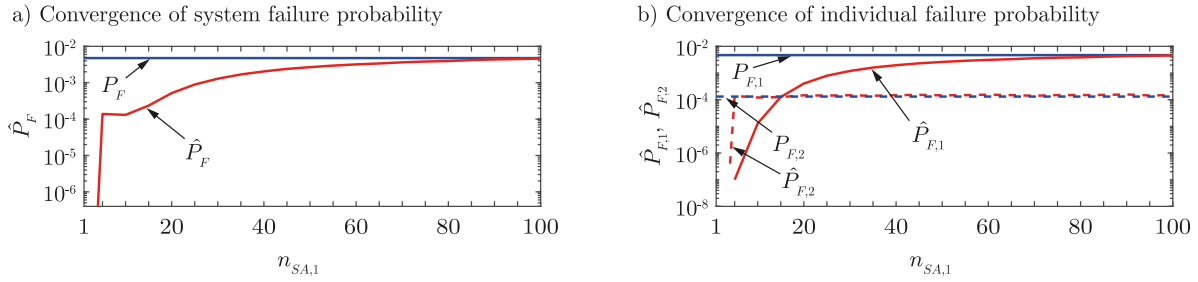

Fig. 18. Failure probability estimates for the sliding failure of the ship lock chamber wall as function of the number of equisized averaging elements in z_1 direction $n_{SA,1}$. Panel a shows the estimate of the system failure probability $\hat{P}_F$ (red line) and panel b shows the estimates of the individual failure probabilities $\hat{P}_{F,1}$ (solid red line) and $\hat{P}_{F,2}$ (dashed red line). The blue lines mark the corresponding reference failure probabilities P_F, $P_{F,1}$ and $P_{F,2}$ (dashed blue line). (For interpretation of the references to color in this figure legend, the reader is referred to the web version of this article.)

Table 5
Effect of the number of SA elements in z_2 direction $n_{SA,2}$ on the failure probability estimate $\hat{P}_F$ for sliding failure of the ship lock chamber, exemplarily for $n_{SA,1} = 25$, $n_{SA,1} = 50$ and $n_{SA,1} = 75$.

$n_{SA,1}$	$\hat{P}_F$		
	$n_{SA,2} = 1$	$n_{SA,2} = 2$	$n_{SA,2} = 3$
25	8.9×10^{-4}	8.4×10^{-4}	8.4×10^{-4}
50	2.7×10^{-3}	2.6×10^{-3}	2.6×10^{-3}
75	3.8×10^{-3}	3.7×10^{-3}	3.6×10^{-3}

P_F for small $n_{SA,1}$. The system failure probability can be split up into the two individual failure probabilities $P_{F,1}$ and $P_{F,2}$ for failure as defined by Eqs. (45) and (47), respectively. Panel b of Fig. 18 shows the convergence of the individual probability estimates $\hat{P}_{F,1}$ (solid red line) and $\hat{P}_{F,2}$ (dashed red line) to the reference solution (respective blue lines) with increasing $n_{SA,1}$. For $n_{SA,1} < 5$ (4), the estimated individual failure probability for failure mechanism 1 (2) is 0. The required number of averaging elements for obtaining a good approximation of $P_{F,1}$ is significantly larger than for $P_{F,2}$. This is related to the nature of the two considered failure mechanisms. $g_1(z_1, \tau(\boldsymbol{z}))$ describes a failure mechanism that is located at a single point in direction z_1, i.e., it is sensitive to local spatial variability. $g_2\left(\bar{z}_1, \tau(\boldsymbol{z})\right)$ on the other hand describes the average resistance over the length $\bar{z}_1$, which is dominated by regions of high and low values of the friction coefficient. This type of failure mechanism is less sensitive to local variations of the RF approximation error, and thus, can be well approximated with a smaller number of averaging elements. Increasing the number of elements in z_2 direction has a minor effect on the estimated failure probability, as shown in Table 5 for $n_{SA,1} = 25$, $n_{SA,1} = 50$ and $n_{SA,1} = 75$. The reason is that both failure mechanisms include an integration of the sliding resistance over W in z_2 direction. The minor changes in $\hat{P}_F$ can be attributed to the fact that $\tau''(\boldsymbol{z})$ is approximated by the geometric average in each SA element. Increasing the number of elements leads to a smaller difference between the integration of geometric averages (with SA) and the integration of $\tau''(\boldsymbol{z})$ (in the reference solution).

This example shows that, for an efficient reliability analysis, the number of SA elements should be chosen depending on the problem at hand. Local failure mechanisms require a larger number of averaging elements than failure mechanisms dominated by averages over specific regions or even determined by global averages. By an intelligent choice of the SA mesh, the stochastic dimension, i.e., the number of random variables, can be significantly reduced without loss of accuracy. This is of special interest in multi-dimensional settings, where on the one hand the number of random variables increases exponentially when the SA mesh is refined and on the other hand, as illustrated above, the SA mesh might need to be fine in one direction but can be relatively coarse in the other direction(s).

4. Conclusion

This paper presents the spatial averaging method for discretizing non-homogeneous random fields with focus on application in reliability analysis with forward engineering models. Non-homogeneous random fields can be induced through a spatial Bayesian update of the random field with measurement data. Each random variable in the discretization with spatial averages represents the average behavior of the random field in a chosen linear (in one dimension) or rectangular (in higher dimensions) spatial domain. Equations to calculate the mean vector and the covariance matrix of the set of averaging random variables are presented. These equations enable direct application of the method to Gaussian random fields. Additionally, we present application of the method to non-Gaussian translation fields and derive the required transformation for fields with lognormal, Student's t- and log-Student's t-marginal distribution.

The performance of the method is investigated through two numerical examples, a one-dimensional beam and a two-dimensional ship lock chamber wall. Thereby, the method is assessed in terms of its ability to accurately represent output quantities of interest and, particularly, the reliability of engineering structures. It is shown that the spatial averaging method is suitable to approximate non-homogeneous random fields with a relatively small set of random variables, especially when the numerical model of the system response involves integration of

the spatially variable quantity. In such cases, even a single random variable can be sufficient for obtaining a reasonable approximation of the output variability. The examples highlight that understanding of the mechanical model is essential for efficient application of the spatial averaging method in conjunction with structural models. It is shown that not only the number of averaging elements but also the size of the individual elements are critical parameters for the performance of the method. An adaptive element size can increase the accuracy of the discretization by increasing the quality of the random field discretization in regions of special importance. However, it cannot be recommended for general application as it requires detailed knowledge of the effect of spatial variability in the input on the output quantity of interest. Thus, a uniform mesh size is to be preferred since it is more robust in terms of the approximation error of the random field discretization. In the absence of an insight on the mechanical model, the number of elements can be chosen by defining a target average relative bias and variance error on the input random field.

The method is particularly suitable for coupling with black box models of engineering systems, such as finite element models, and, hence, enables consideration of spatial variability in practical reliability analyses. Additionally, the presented method can be used to account for spatial variability in the verification of structures, e.g., by determining a conservative estimate for the spatial average of material properties or by accounting for spatial load bearing behavior but still maintaining the simplifications of a plane structural model. It is left to future studies to investigate the suitability of the spatial averaging method for practical application in structural verification.

CRediT authorship contribution statement

Sebastian Geyer: Conceptualization, Methodology, Software, Investigation, Writing – original draft, Visualization. **Iason Papaioannou:** Conceptualization, Methodology, Writing – review & editing, Supervision. **Lori Graham-Brady:** Conceptualization, Writing – review & editing, Supervision. **Daniel Straub:** Conceptualization, Methodology, Writing – review & editing, Supervision, Project administration, Funding acquisition.

Declaration of competing interest

The authors declare that they have no known competing financial interests or personal relationships that could have appeared to influence the work reported in this paper.

Acknowledgments

This work has been financially supported by the *Bundesanstalt für Wasserbau* (Federal Waterways Engineering and Research Institute, Germany). The corresponding author would like to thank Claus Kunz from the *Bundesanstalt für Wasserbau* for discussions that have considerably enhanced the quality of the paper.

References

[1] Geyer S, Papaioannou I, Kunz C, Straub D. Reliability assessment of large hydraulic structures with spatially distributed measurements. Struct Infrastruct Eng 2020;16(4):599–612.
[2] Phoon K-K, Kulhawy FH. Characterization of geotechnical variability. Can Geotech J 1999;36(4):612–24.
[3] Savvas D, Papaioannou I, Stefanou G. Bayesian identification and model comparison for random property fields derived from material microstructure. Comput Methods Appl Mech Engrg 2020;365:113026.
[4] Vanmarcke E. Random fields: Analysis and synthesis, revised and expanded new edition. World Scientific; 2010.
[5] Sudret B, Der Kiureghian A. Stochastic finite element methods and reliability. A state-of-the-art report. Report on Research No. UCB/SEMM-2000/08, Berkeley: University of California; 2000.
[6] Liu Y, Li J, Sun S, Yu B. Advances in Gaussian random field generation: a review. Comput Geosci 2019;1–37.
[7] Vanmarcke E, Grigoriu M. Stochastic finite element analysis of simple beams. J Eng Mech 1983;109(5):1203–14.
[8] Rackwitz R. Reviewing probabilistic soils modelling. Comput Geotech 2000;26(3):199–223.
[9] Fenton GA, Griffiths DV. Bearing-capacity prediction of spatially random $c-\phi$ soils. Can Geotech J 2003;40(1):54–65.
[10] Fenton GA, Griffiths DV. Three-dimensional probabilistic foundation settlement. J Geotech Geoenviron Eng 2005;131(2):232–9.
[11] Ching J, Tong X-W, Hu Y-G. Effective Young's modulus for a spatially variable soil mass subjected to a simple stress state. Georisk Assess Manage Risk Eng Syst Geohazards 2016;10(1):11–26.
[12] Tabarroki M, Ching J, Phoon K-K, Chen Y-Z. Mobilisation-based characteristic value of shear strength for ultimate limit states. Georisk Assess Manage Risk Eng Syst Geohazards 2021;1–22.
[13] Vanmarcke E, Shinozuka M, Nakagiri S, Schuëller G, Grigoriu M. Random fields and stochastic finite elements. Struct Saf 1986;3(3):143–66.
[14] Der Kiureghian A, Ke J-B. The stochastic finite element method in structural reliability. Probab Eng Mech 1988;3(2):83–91.
[15] Graham L, Deodatis G. Variability response functions for stochastic plate bending problems. Struct Saf 1998;20(2):167–88.
[16] Vořechovský M, Eliáš J. Fracture in random quasibrittle media: Ii. Analytical model based on extremes of the averaging process. Eng Fract Mech 2020;235:107155.
[17] Zhu WQ, Ren YJ, Wu WQ. Stochastic FEM based on local averages of random vector fields. J Eng Mech 1992;118(3):496–511.
[18] Geyer S, Papaioannou D, Straub I, Kunz C. Bayesian reliability assessment with spatially variable measurements: the spatial averaging approach. In: Song J, editor. Proceedings of the 13th international conference on application of statistics and probability in civil engineering. Seoul: Seoul National University open repository; 2019, p. 1–8.
[19] Papaioannou I, Geyer S, Straub D. Bayesian updating of foundation reliability with spatially variable measurements: a spatial averaging approach. In: Ching J, Li DQ, Zhang J, editors. Proceedings of the 7th international symposium on geotechnical safety and risk. Research publishing; 2019, p. 619–24.
[20] Fenton GA. Random field modeling of CPT data. J Geotech Geoenviron Eng 1999;125(6):486–98.
[21] Ching J, Phoon K-K. Characterizing uncertain site-specific trend function by sparse Bayesian learning. J Eng Mech 2017;143(7):04017028.
[22] Gelman A, Carlin J, Stern H, Dunson D, Vehtari A, Rubin D. Bayesian data analysis. Chapman & Hall/CRC texts in statistical science, 3rd ed.. Boca Raton, FL: Taylor & Francis; 2013.
[23] Papaioannou I, Straub D. Learning soil parameters and updating geotechnical reliability estimates under spatial variability – theory and application to shallow foundations. Georisk Assess Manage Risk Eng Syst Geohazards 2017;11(1):116–28.
[24] Uribe F, Papaioannou I, Betz W, Straub D. Bayesian inference of random fields represented with the Karhunen–Loève expansion. Comput Methods Appl Mech Engrg 2020;358:112632.
[25] Stein M. Interpolation of spatial data: Some theory for kriging. Springer series in statistics, New York City, NY: Springer; 1999.
[26] Spanos P, Ghanem R. Stochastic finite element expansion for random media. J Eng Mech 1989;15(5):1035–53.
[27] Ghanem RG, Spanos PD. Stochastic finite elements. A spectral approach, revised edition. Dover civil and mechanical engineering, Mineola, NY: Dover; 2012.
[28] Fenton GA, Vanmarcke EH. Simulation of random fields via local average subdivision. J Eng Mech 1990;116(8):1733–49.
[29] Grigoriu M. Existence and construction of translation models for stationary non-Gaussian processes. Probab Eng Mech 2009;24(4):545–51.
[30] Geyer S, Papaioannou I, Straub D. Bayesian analysis of hierarchical random fields for material modeling. Probab Eng Mech 2021;66:103167.
[31] Abrahamsen P. A review of Gaussian random fields and correlation functions. 2nd ed.. Norwegian Computing Center; 1997.
[32] Li C, Kiureghian AD. Optimal discretization of random fields. J Eng Mech 1993;119(6):1136–54.
[33] Grigoriu M. Stochastic systems: Uncertainty quantification and propagation. Springer series in reliability engineering, London: Springer; 2012.
[34] Knabe W, Przewłócki J, Różyński G. Spatial averages for linear elements for two-parameter random field. Probab Eng Mech 1998;13(3):147–67.
[35] Matthies HG, Brenner CE, Bucher CG, Guedes Soares C. Uncertainties in probabilistic numerical analysis of structures and solids - stochastic finite elements. Struct Saf 1997;19(3):283–336.
[36] Grigoriu M. Crossings of non-Gaussian translation processes. J Eng Mech 1984;110(4):610–20.
[37] Liu P-L, Kiureghian AD. Multivariate distribution models with prescribed marginals and covariances. Probab Eng Mech 1986;1(2):105–12.
[38] Bishop CM. Pattern recognition and machine learning, information science and statistics. New York City, NY: Springer; 2006.
[39] Kotz S, Nadarajah S. Multivariate t-distributions and their applications. Cambridge University; 2004.

[40] Vanegas LH, Paula GA. Log-symmetric distributions: statistical properties and parameter estimation. Braz J Probab Stat 2016;30(2):196–220.
[41] Betz W, Papaioannou I, Straub D. Numerical methods for the discretization of random fields by means of the Karhunen–Loève expansion. Comput Methods Appl Mech Engrg 2014;271:109–29.
[42] European Committee for Standardization. EN 1992-1-1:2004-12: Eurocode 2: Design of concrete structures - Part 1-1: General rules and rules for buildings. European standard, European Committee for Standardization; 2004.
[43] Bundesanstalt für Wasserbau. Bewertung der Tragfähigkeit bestehender, massiver Wasserbauwerke [Assessment of the bearing capacity of existing, massive hydraulic structures]. Karlsruhe, Germany: BAW guideline, Bundesanstalt für Wasserbau; 2016.
[44] Rasmussen C, Williams C. Gaussian processes for machine learning. Adaptive computation and machine learning, Cambridge, MA: MIT; 2006.